PERGAMON

Quaternary Science Reviews 19 (2000) 1543–1562

QSR

Southern Alaska as an example of the long-term consequences of mountain building under the influence of glaciers

Andrew Meigs[a,*], Jeanne Sauber[b]

[a]Department of Geosciences, Oregon State University, 104 Wilkinson Hall, Corvallis, OR 97331, USA
[b]NASA, Goddard Space Flight Center, Geodynamics Branch, Code 921, Greenbelt, MD 02139, USA

Abstract

Southern Alaska is a continent-scale region of ongoing crustal deformation within the Pacific–North American plate boundary zone. Glaciers and glacial erosion have dictated patterns of denudation in the orogen over the last ~ 5 Myr. The orogen comprises three discrete topographic domains from south to north, respectively: (1) the Chugach/St. Elias Range; (2) the Wrangell Mountains; and (3) the eastern Alaska Range. Although present deformation is distributed across the orogen, much of the shortening and uplift are concentrated in the Chugach/St. Elias Range. A systematic increase in topographic wavelength of the range from east to west reflects east-to-west increases in the width of a shallowly dipping segment of the plate interface, separation of major upper plate structures, and a decrease in the obliquity of plate motion relative to the plate boundary. Mean elevation decays exponentially from ~ 2500 to ~ 1100 m from east to west, respectively. Topographic control on the present and past distribution of glaciers is indicated by close correspondence along the range between mean elevation and the modern equilibrium line altitude of glaciers (ELA) and differences in the modern ELA, mean annual precipitation and temperature across the range between the windward, southern and leeward, northern flanks. Net, range-scale erosion is the sum of (1) primary bedrock erosion by glaciers and (2) erosion in areas of the landscape that are ice-marginal and are deglaciated at glacial minima. Oscillations between glacial and interglacial climates controls ice height and distribution, which, in turn, modulates the locus and mode of erosion in the landscape. Mean topography and the mean position of the ELA are coupled because of the competition between rock uplift, which tends to raise the ELA, and enhanced orographic precipitation accompanying mountain building, which tends to lower the ELA. Mean topography is controlled both by the 60° latitude and maritime setting of active deformation and by the feedback between shortening and uplift, glacial erosion, and orographic effects on climate accompanying mountain building.

1. Introduction

Speculation that mountain building may be linked with climate change (Molnar and England, 1990; Raymo and Ruddiman, 1992), and models that suggest erosional patterns may influence deformation (Beaumont et al., 1992, 1996; Royden, 1993; Koons, 1994, 1998; Huerta et al., 1996), has focused attention on the linkages between topographic form, patterns of deformation, and modes of erosion in active orogenic systems. Which aspects of landscape form, however, are related to deformational patterns and which are erosionally controlled is not clear in detail. High peaks and large relief impress a lasting image of the topography at active continental margins (Masek et al., 1994). The highest peaks are dramatic and typically emerge above the rest of the landscape in descriptions of the topography of these ranges. That the peaks correlate with underlying structure (i.e. major thrust faults), is commonly inferred from thermochronometric and other data (Seeber and Gornitz, 1983; Zeitler, 1985; Molnar, 1987; Gilchrist et al., 1994; O'Sullivan and Currie, 1996; Zeitler and Koons, 1998). If topographic texture, such as the distribution of peaks, is related to structure first, topographic change at wavelengths extending from the spacing of structures to that of the full orogen must be controlled by deformational patterns.

In the northwest Himalaya, however, an active orogen characterized by bedrock uplift rates of 5–10 mm/yr locally (Zeitler et al., 1982; Zeitler, 1985; Burbank et al., 1996), regional uplift patterns do not adequately explain range-scale topographic variations (Brozovic et al., 1997). A north-trending structural grain, dramatic topographic relief, and a suite of ~ 8000 m peaks (Nanga Parbat, Haramosh, and others), characterizes the region

* Corresponding author. Tel.: +1-541-737-1214; fax: +1-541-737-1200.

E-mail addresses: meigsa@geo.orst.edu (A. Meigs), jeanne@steller.gsfc.nasa.gov (J. Sauber).

0277-3791/00/$ - see front matter
PII: S0277-3791(00)00077-9

(Zeitler et al., 1989; Seeber and Pecher, 1998). Topographic measures, including mean elevation and hypsometry (area/altitude distribution), indicate that areas characterized by rapid uplift ($\geqslant 5$ mm/yr) cannot be differentiated from adjacent domains with substantially lower rates ($\leqslant 1$ mm/yr) on the basis of topography (Brozovic et al., 1997). Fifty percent of the surface area and the mean elevation are within the altitudinal range of equilibrium line altitudes (ELA), of glaciers today and those estimated for the last glacial maximum. Mean elevation and area-altitude distribution track a northward, climatically controlled rise in the ELA; a trend that is at a high angle to structural trend. These observations suggest that the northwest Himalayan topography is controlled primarily by the mean position of the ELA in space and time. That control is an extension of the argument that glacial erosion rate scales with glacier sliding velocity (Andrews, 1972; Hallet, 1979; Humphrey and Raymond, 1994). Sliding velocity is related to ice flux, which reaches a maximum at the ELA (Andrews, 1972). Thus, glacial erosion is inferred to be particularly efficient in the elevation range of the ELA.

One implication of the hypothesis that erosional patterns are linked to the ELA is that erosional processes must vary as a function of variations in glacial coverage of the landscape (Porter, 1989b). ELA lowering during glacial epochs is accompanied by extension of glaciers down-valley (Fig. 1). Interglacial periods are marked by an elevated ELA and retracted glacial positions throughout the landscape. Valley walls and bottoms are alternately covered and uncovered by glaciers as climate shifts between glacial and interglacial states. Roughly equal amounts of the past two million years were glacial and interglacial (Williams et al., 1988), and glaciers, on average, were more extensive than they are at present (Porter, 1989b). Mean, orogen-scale 'glacial erosion' involves primary glacial erosion of bedrock (Andrews, 1972; Hallet, 1979; Harbor, 1992; Hallet et al., 1996), as well as erosion in ice-marginal and ice-free portions of the landscape. The later erosion is modulated by glacier distribution in space and time (Church and Ryder, 1972; Church and Slaymaker, 1989; Sidle and Milner, 1989; Harbor and Warburton, 1993; Meigs, 1998). Thus, erosional modification of topography occurs via a different suite of processes at full glacial, full interglacial, and during transition between the two climate states.

Subsidence or uplift of the solid Earth also accompanies climatic oscillations in glacial extent; a decrease in ice mass that occurs during glacial retreat would result in uplift of the solid Earth (Sauber et al., 1999). These ice thickness changes are largest near the glacier terminus. Near Icy Bay, for example, uplift due to the Earth's viscoelastic response to terminus retreat and ice thinning this century may be as high as 1–2 cm/yr. In this

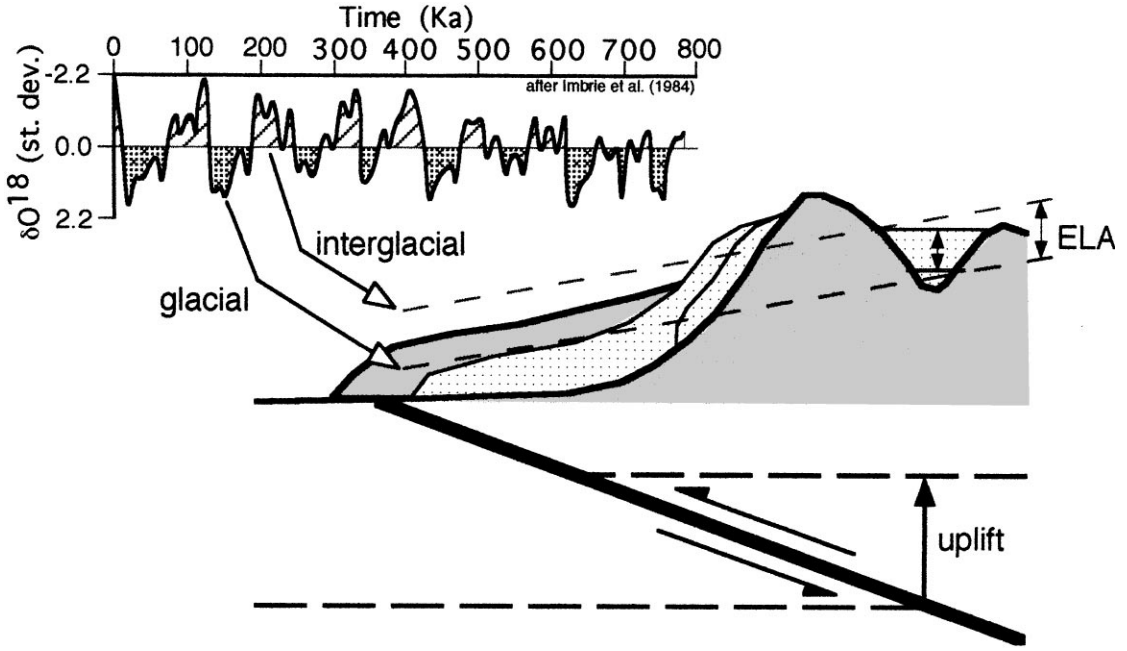

Fig. 1. Conceptual model illustrating the uplift by structures at depth and position of the equilibrium line altitude (ELA) of glaciers in the landscape. Depression and elevation of the ELA is a function of the magnitude of glacial and interglacial periods, which dictate the mean position of the ELA (Porter, 1989b). Changes in the magnitude to which ice extends down-valley and covers valley walls are proportionate to climatic oscillations. The solid Earth response to climate-induced change in glacial extent is expected to be subsidence at glacial maxima, due to increased ice mass, and uplift during interglacial periods due to mass reduction/removal. Shaded area marks bedrock at base of glaciers and on valley walls parallel to glacial valley. Light stippled area denotes glacial extent during full glacial conditions, the line inset within the stippled area depicts a reduced interglacial extent. Oxygen isotope curve is from Imbrie et al. (1984). Glacial periods are shaded, interglacial periods are cross-hatched.

dominantly thrust earthquake environment, ice loading during glacial advances tends to increase the vertical stress, σ3, implying that earthquakes may be less likely. During glacial retreat, in contrast, σ3 decreases and failure in earthquakes is more likely.

Arguing that topography is controlled by the ELA runs contrary to the view that topography controls the ELA (Østrem, 1972; Péwé, 1975; Porter, 1975, 1977; Østrem et al., 1981; Porter et al., 1983). Close correspondence between topographic details (including strike of major ranges and position of topographic saddles and crests), and isoglacihypses (contours of the glaciation threshold), represents the primary observation used to infer a topographic control on glacier distribution. Departures of the glaciation threshold from the expected altitudinal position for a region, based on latitude, precipitation patterns, and inferred surface temperature lapse rates, has been argued to provide evidence for tectonic uplift or lowering of the glaciation threshold (Péwé, 1975; Porter et al., 1983). Such an inference implies that glacial erosion rates do not keep pace with uplift rates. Sediment yield data from Alaskan and other glaciers, in contrast, suggest that glacial erosion rates (>10 mm/yr; Hallet et al., 1996), are of the same order as the highest rock uplift rates measured in active orogenic belts. These data allude to the possibility that glacial erosion can match or exceed rock uplift rates.

Questions central to unravelling the relationships between climate, glaciers, and tectonics in setting the topographic form of active orogenic belts include:

- What is the topographic form of an active orogenic belt whose erosion has been dominated by glaciers?
- How do topographic characteristics relate to tectonic and climatic patters?
- What is 'mean glacial erosion'? How do erosional patterns and processes vary with climatically forced oscillations in ice distribution?
- Can a climatic control on the landscape be differentiated uniquely from a tectonic control?

We have integrated a topographic analysis of a digital elevation model of southern Alaska with simple models of crustal deformation, estimates of the ELA regionally, new field data from a recently deglaciated portion of the landscape, and models of past glacial coverage of the landscape. Southern Alaska is nearly ideal for such an analysis because deformation over the last ~ 5 Myr has been accompanied by glaciation (Plafker, 1987; Eyles et al., 1991; Lagoe et al., 1993), new geodetic data provide good constraints on the modern deformation field (Sauber et al., 1997), seismic data constrain the orientation and depth of many of the major structures (Page et al., 1989; Eastabrook et al., 1992; Plafker et al., 1994a), present regional climatic trends, including the ELA, are adequately constrained (Mayo, 1986), and the region has experienced significant and well-documented glacial retreat over the last century (Tarr, 1909; Miller, 1961; Mann and Ugolini, 1985; Molnia, 1986; Porter, 1989a).

2. Crustal deformation in Southern Alaska

Located along the Pacific–North American plate boundary at the syntaxial bend from northwestern to western trends in major structures, southern Alaska consists of a bedrock assemblage accreted to North America in the Mesozoic and Cenozoic (Fig. 2) (Plafker, 1987; Plafker et al., 1994a). Plate motion studies, GPS geodesy, and finite element modelling indicate that roughly two-thirds of the ~ 53 mm/yr Pacific–North American plate motion is accommodated across a diffuse zone extending from offshore more than 200 km northward into interior Alaska (Lahr and Plafker, 1980; Plafker et al., 1994a; Lundgren et al., 1995; Bird, 1996; Sauber et al., 1997). Deformation is on-going, driven by the combination of

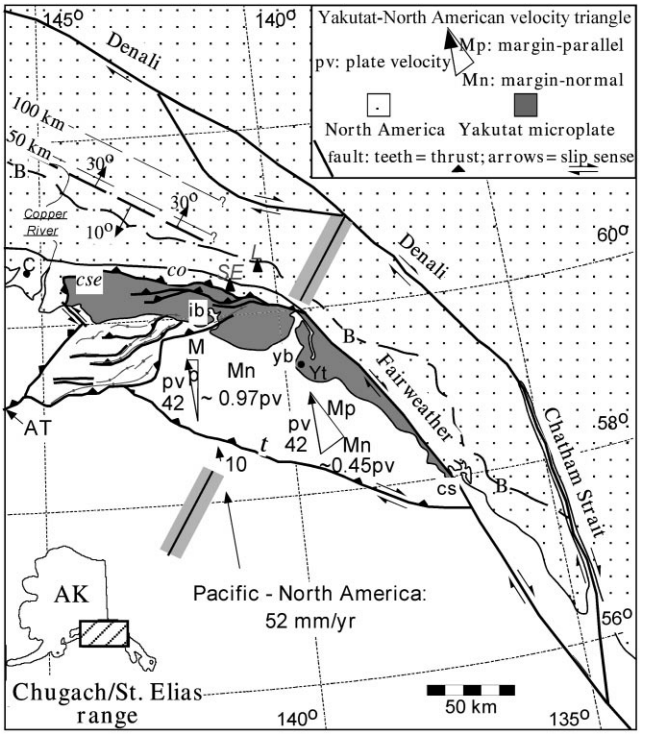

Fig. 2. Major structures, structural trends, and velocity vectors across the actively deforming southern margin of Alaska (Plafker, 1987; Page et al., 1989; Plafker et al., 1994a). The northeast-treading line denotes the transition from the southeastern region where margin-parallel (Mp, in% pv) motion is a significant component of the plate vector (pv) from that region to the west where the margin-normal (Mn, in%pv) is the dominant component. Mts. Logan (L; 6050 m) and St. Elias (SE; 5490 m) are indicated. C denotes Cordova, Yt is Yakutat, ib is Icy Bay, yb is Yakutat Bay, cs is Cross Sound, AT is the Aleutian trench, cse is the Chugach/St. Elias thrust, and B is the Border Ranges fault. 50, 100 km, and a change in dip from 10 to 30° are indicated for the subducting Pacific Plate.

Pacific–North American plate interaction and by the accretion and underthrusting of the Yakutat microplate beneath North America (Plafker, 1987; Plafker et al., 1994b). Evidence of this deformation includes historical seismicity, accumulating interseismic strain, uplifted marine terraces and deformed moraines, actively deforming geological structures, and Pliocene and younger apatite fission-track cooling ages (Tarr and Martin, 1912; Hudson et al., 1976; Plafker et al., 1978, 1982, 1994a, b; Lahr and Plafker, 1980; Mann and Ugolini, 1985; Bruns and Carlson, 1987; Plafker, 1987; O'Sullivan and Currie, 1996; O'Sullivan et al., 1997; Sauber et al., 1997, 1999; Eyles and Lagoe, 1998). In detail, plate motion is transferred through the syntaxial bend from a single northwest-treading strike-slip fault system (Queen Charlotte/Fairweather) to a series of reverse and oblique-slip faults from east to west, respectively. Simple decomposition of the plate motion vector illustrates that upper-plate crustal deformation within the Yakutat terrane and North America changes as a function of a substantial decrease in the margin-parallel component of plate motion from east to west, respectively (Fig. 2).

The principle structural elements are, from south to north (Fig. 2): (1) the Fairweather fault (south of Cross Sound), Transition fault, and Aleutian Trench, which collectively define the plate boundary with the Pacific Plate; (2) the Fairweather fault (north and west of Cross Sound) and Chugach/St. Elias thrust, which define the eastern and northern margins of the Yakutat terrane; (3) the Chitina-Copper River valley, a major topographic low that coincides with a change from 10 to 30° in the dip of the Pacific–North American plate interface; and (4) the Chatham Strait/Denali fault system. Fault slip rates on the principal faults are not well-constrained geologically. Approximately, 10 mm/yr are inferred to be accommodated by the Transition fault (Bruns and Carlson, 1987; Plafker et al., 1994a), although best-fit finite element models of regional deformation imply that this fault is inactive (Lundgren et al., 1995). Internal deformation by imbricate thrust faults within the Yakutat terrane absorb an unconstrained amount of crustal shortening. Direct estimates of slip rate on the Chugach/St. Elias thrust system are elusive. Models of neotectonic deformation of Alaska suggest horizontal rates between 20 and 30 mm/yr (Lundgren et al., 1995; Bird, 1996). Geologically constrained slip rates for the Denali fault system are $\sim$ 8–12 mm/yr (Plafker et al., 1977). Geodetically constrained rates are lower (2–5 mm/yr; Sauber et al., 1997). Current GPS geodesy across the plate boundary is consistent with this overall northward decay in fault slip rate, although they lack sufficient spatial density to resolve slip on individual fault segments (Sauber et al., 1997, 1999). Elastic modelling of these data suggests that the interface between the upper plate and down-going Pacific plate is locked from approximately the Pamplona zone to the Contact fault (Fig. 2).

In the area of this study (west of $\sim$ 140° longitude), the structural trend changes from predominantly northeast- to east-treading near the coast to northwest-trending from the Chitina-Copper River valley north (Fig. 2). Principle topographic elements reflect this regional structural fabric (Fig. 3a). Three discrete topographic domains, the Chugach/St. Elias Range, the Wrangell Mountains, and the eastern Alaska Range, can be differentiated from south to north, respectively (Figs. 3 and 4). The Chugach/St. Elias Range extends from the coast to the Chitina-Copper River valley and includes the onshore portion of the Yakutat terrane, the Chugach/St. Elias, Contact, and Border Ranges faults, and the two highest peaks in the study area, Mt. St. Elias (5490 m) and Mt. Logan (6050 m). A dramatic set of high stratovolcanoes ($\sim$ 4000–5000 m summits) cap the northwest-treading Wrangell Mountains (Miller and Richter, 1994). Structure contours on the down-going Pacific Plate inferred from seismicity (Page et al., 1989), and alignment of the volcano summits suggest that the strike of the down-going plate is northwest (Fig. 3). The Chitina-Copper River Valley coincides with the surface projection of the axial surface created at the bend in the Pacific Plate at depth inferred from seismicity data and elastic modelling of GPS data (Sauber et al., 1997). Lying to the north of the Wrangell Mountains across the Denali-Totschunda fault, the eastern Alaska Range is topographically subdued in comparison with the ranges to the south. A broad low-relief plain defines the northwestern topographic boundary of the eastern Alaska Range. The Denali fault cuts obliquely across the eastern Alaska Range; the fault lies near the southern boundary in the west, but defines the northern boundary in the east.

3. Landscape morphometric analysis

Topographic characteristics were measured for the region of the Pacific–North American plate boundary between $\sim$ 140–145° W longitude and $\sim$ 59°45′—64° N latitude (Fig. 3). Characterization of regional trends in topographic form, hypsometry, mean elevation, and slope were the objectives of this analysis. These analyses quantify the form of the landscape and serve as the means by which linkages between the modern plate-boundary deformation field, long-term patterns of crustal deformation, and the temporal and spatial distribution and fluctuation of glaciers are investigated.

3.1. Methods

A digital elevation model (DEM) for southern Alaska was compiled from USGS data (see Fig. 3 caption for the worldwide web source). These data have $\sim$ 175 m grid spacing and $\pm$ 3 m elevation uncertainty. Mean elevation was calculated within a window of 30×30 data

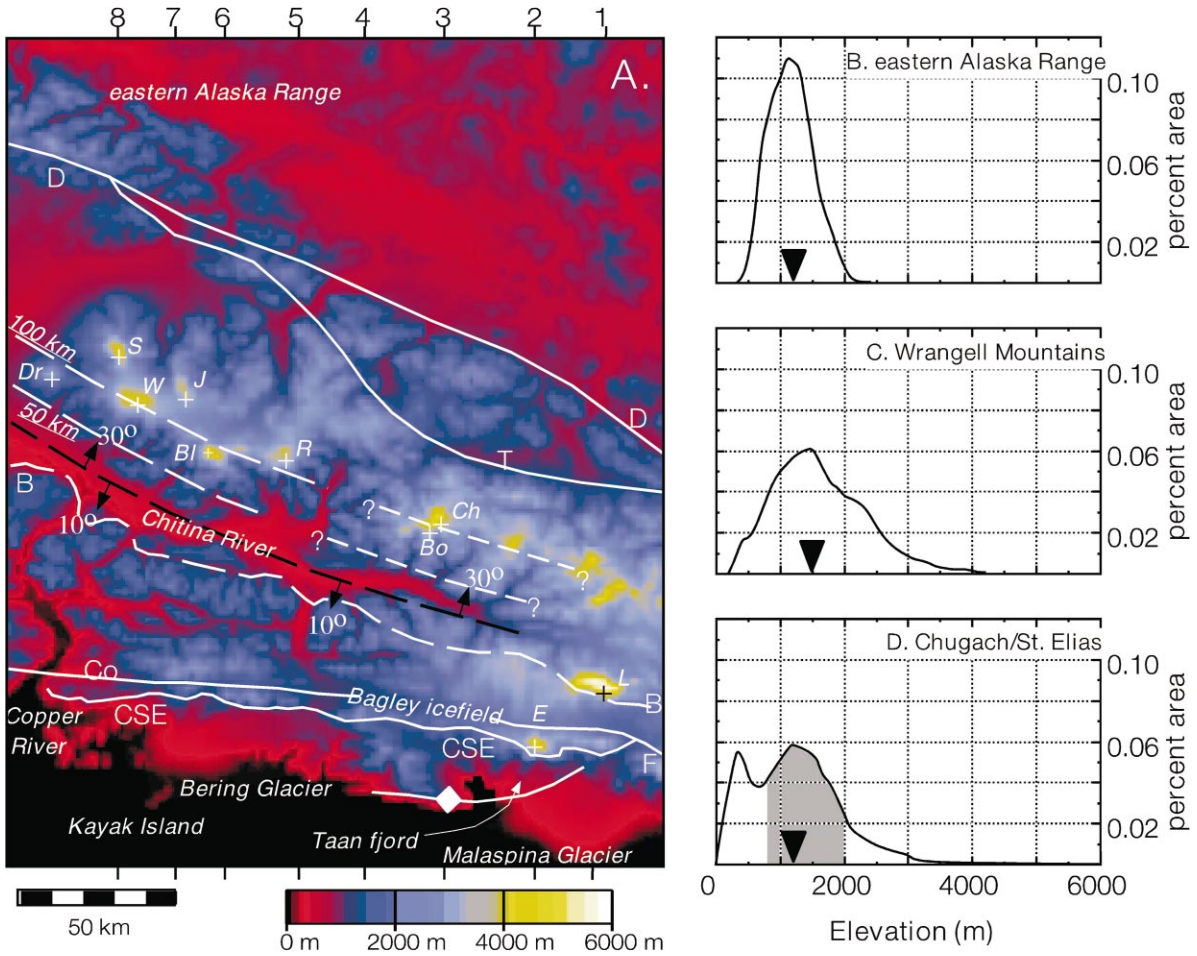

Fig. 3. (a) Major structural elements superimposed on the digital elevation model (DEM) of the study region. The principal structures are the Fairweather fault (F), the deformation front of the Yakutat microplate collision (denoted by an anticlinal fold axis), the Chugach-St. Elias thrust fault (CSE), the Contact fault (Co), the Border Ranges fault (B), the Totschunda fault (T), and the Denali (D) fault from south to north, respectively. Note that the Contact fault coincides with a major glacial trough, the Bagley Ice Field. Other structural features include the 50 and 100 km contours on the top of the down-going Yakutat (Pacific?) plate and the inferred surface position of the transition from 10 to 30° dip (at ~40 km depth) of the down-going plate (black line with offset arrows). The peaks of Mts. St. Elias and Logan are indicated by E and L, respectively. Peaks within the Wrangell Mountains include Mts. Drum (Dr), Sanford (S), Wrangell (W), Jarvis (J), Blackburn (Bl), Regal (R), Bona (Bo), and Churchill (Ch). Hypsometric curves and mean elevation (dark triangle) are plotted for the (b) eastern Alaska Range, (c) Wrangell Mountains, and (d) Chugach/St. Elias Range topographic provinces. A shaded region indicates the altitudinal range of the modern ELA (from Mayo, 1986). The DEM can be obtained from: (edcwww.cr.usgs.gov/Webglis/glisbin/guide.pl/glis/hyper/guide/usgs,dem).

point (~5×5 km) scrolling pixel by pixel across and down the data set. Mean elevation represents the sum of the elevations within a window divided by the number of data points within that window. A plot of the hypsometry of each region accompanies Fig. 3. South–north profiles were extracted from the map of mean elevation at ~30 km intervals across the region (Fig. 4). A smoothed curve of the data comprising each profile are plotted atop the original profile. The smoothing function averages elevations within ±10% of the data range (~150 points) of an individual elevation point. Thus, the smoothed data reflects long-wavelength topographic variation (over ~50–100 km) whereas the mean elevation data highlights short-wavelength relief (over ~10's km).

Slope was also calculated within a scrolling window (5×5 data points). A least-squares best-fitting plane was determined for each window and the angle of that plane from horizontal was measured as a proxy for slope. Slope calculated from DEM data consistently underestimates slope inversely with respect to grid spacing, i.e. large grid spacing (90 m or greater) reveals lower slope, higher slope angles are calculated using data with smaller grid spacing (Zhang and Montgomery, 1994). Slope is plotted by altitude and includes the 25th, 50th, and 75th percentile slope distributions for 100 m altitude bins (Fig. 6b–d). A smoothed curve of the original curve comprising each slope/altitude curve are plotted. The smoothing function averages slope within ±10% of the data range of a slope estimate.

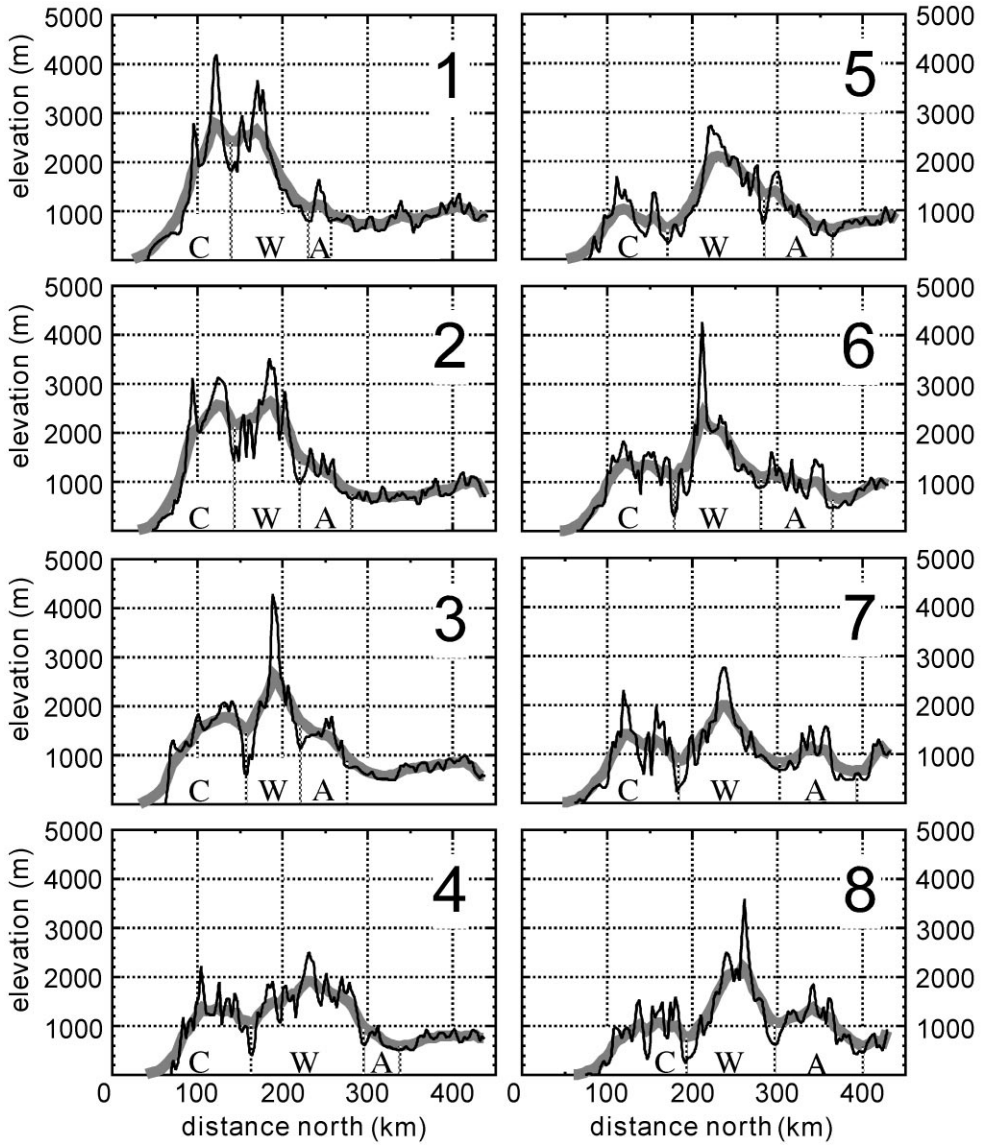

Fig. 4. Serial north–south topographic profiles from east (1) to west (8) spaced ~ 30 to 50 km apart. Included are the topographic profiles for each transect (see text for discussion of smoothing). C,W, and A denote the Chugach/St. Elias Range, Wrangell Mountains, and eastern Alaska Range domains, respectively. The profiles have 50× vertical exaggeration. Zero km lies on the south. The coast on most profiles falls 25–50 km north of 0 km on the *x*-axis.

3.2. Results

Eight south–north profiles were extracted from the mean elevation map in order to characterize topography across the region (Figs. 4 and 5). Three general trends in the form of the landscape can be seen by comparing profiles across the region. A broad (100 km), high (2500 m) region consisting of the Chugach/St. Elias and Wrangell domains dominates the topography in the east (profiles 1 and 2, Fig. 4). On the west, in contrast, the regional topography has ~ 150 km wavelength that varies about ~ 1100 m elevation and individual maxima in each domain (1000 m, Chugach/St. Elias; 2000 m, Wrangell Mountains; and 1100 m, eastern Alaska Range; profiles 7 and 8, Fig. 4). Thus, topographic wavelength and amplitude appear to change from east to west. Moreover, the topographic domains are increasingly distinct from east and west, the spatial separation between which is marked by the appearance of large strike-parallel valleys. Much of the topographic change correlates with changes in the geometry of the plate interface and in major bedrock structures (Fig. 3a). The broader width appears to correspond with an increase in the width of the shallow segment of the plate interface, as indicated by the distance between the coast and the 50 km contour on the down-going plate. The appearance of the major valleys

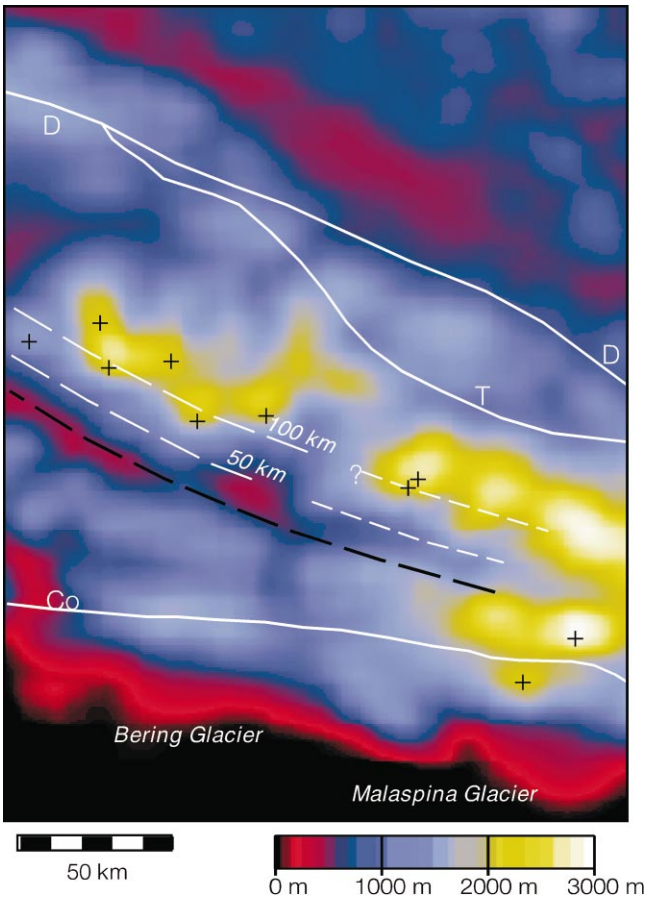

Fig. 5. Map of mean elevation with selected major structures and topographic features from Fig. 3 plotted for reference. See text for discussion of window size and methodology.

reflects the westward fanning of major upper plate structures.

When the mean height of the Chugach/St. Elias Range on each of the eight profiles is plotted on an east–west profile, an apparent westward exponential decay in range elevation is revealed (Figs. 5 and 9). A steady decrease in elevation is seen between profile 1 on the east and profile 4–100 km to the west. From profile 4 west, range height does not seem to vary systematically, rather it appears to fluctuate within a narrow range between 900 and 1200 m. Profile 5 intersects a north-treading topographic low that is the site of north- and south-draining outlet glaciers from the Bagley Ice Field (Fig. 3a), which may explain its anomalously low elevation in comparison with profiles 4 and 6 to the east and west, respectively. The Copper River, the only transverse drainage across the full width of the Chugach/St. Elais Range, is also marked by a topographic low.

Relief also decreases from east to west, as indicated by the high-frequency curves for each profile (Fig. 4). Relief in the Chugach/St. Elais Range, for example, is as high as 2100 m in the east, whereas 600–800 m is more typical in the west. The highest relief is associated with a series of west to northwest trending topographic lows that are presently occupied by major glaciers or were occupied by glaciers at the last glacial maximum (Fig. 3a). These valleys are also the sites of the major faults in some cases (the Bagley Ice Field coincides with Contact fault, for example). Relief in the Wrangell Mountains and eastern Alaska Range, in contrast, is less variable from east to west. The Wrangell Mountains tend to have a single peak in elevation in each profile (Fig. 4). Most of the individual topographic spikes reflect intersection of the profile with one of the stratovolcanoes in the range. As a distinct topographic entity, the eastern Alaska Range maintains about the same height ($\sim$ 1000 m) and relief ($<$ 600 m) across the study area.

Area/altitude relationships change systematically from south to north (Figs. 3b–d). Altitude in the Chugach/St. Elias Range is bimodally distributed with nearly equal amounts of area at 300 and 1200 m (Fig. 3d). The distribution is strongly affected by the surface elevations of the Bagley Ice Field, the Bering glacier, the Malaspina glacier, other glaciers, and deglaciated valley bottoms. Mean elevation ($\sim$ 1225 m) is low in comparison with the elevation of highest peaks ($>$ 6000 m for Mt. Logan). More importantly, however, is the fact that more than 90% of the land area lies in an altitudinal band between 300 and 2200 m above sea level and that the surface area above 3200 m occupies less than 2% of the landscape. Mean elevation (1475 m) is only slightly lower than the modal elevation (1500 m) in the Wrangell Mountain (Fig. 3c). Altitude is moderately left-skewed as the consequence of the high elevation of each of the Wrangell volcanoes (Fig. 3a). Elevations have an essentially normal distribution in the eastern Alaska Range (Fig. 3b). Although the modal elevation (1100 m) is slightly lower than the mean elevation (1214 m), more than 30% of the area has elevations between 1100 and 1300 m. Peak elevations exceed 2600 m in this part of the Alaska Range. Similar to the Chugach/St. Elias domain, these peaks occupy a small fraction of the surface area. Whereas percent area occupied by high peaks is expected to be small in glacial and fluvial landscapes, differences in valley-bottom form between the two landscapes ought to be reflected in the hypsometry at low elevations (compare Figs. 3b and d; Harbor, 1992; Duncan et al., 1998; Whipple et al., 1999).

Patterns of slope distribution show several interesting trends (Fig. 6). The form of slope/altitude curves for the Chugach/St. Elias and eastern Alaska Range are similar in the $\sim$ 1000–2500 m elevation range. Both are characterized by central plateaus in slope bound by a step to substantially higher slope angles at higher elevations (Figs. 6b and d). A jump from 20–30° to $\sim$ 60° is seen at 3000 m elevation in the Chugach/St. Elias Range. The step is less profound, from 22–28° to nearly 40°, and occurs at a lower elevation, 2000 m, in the eastern Alaska

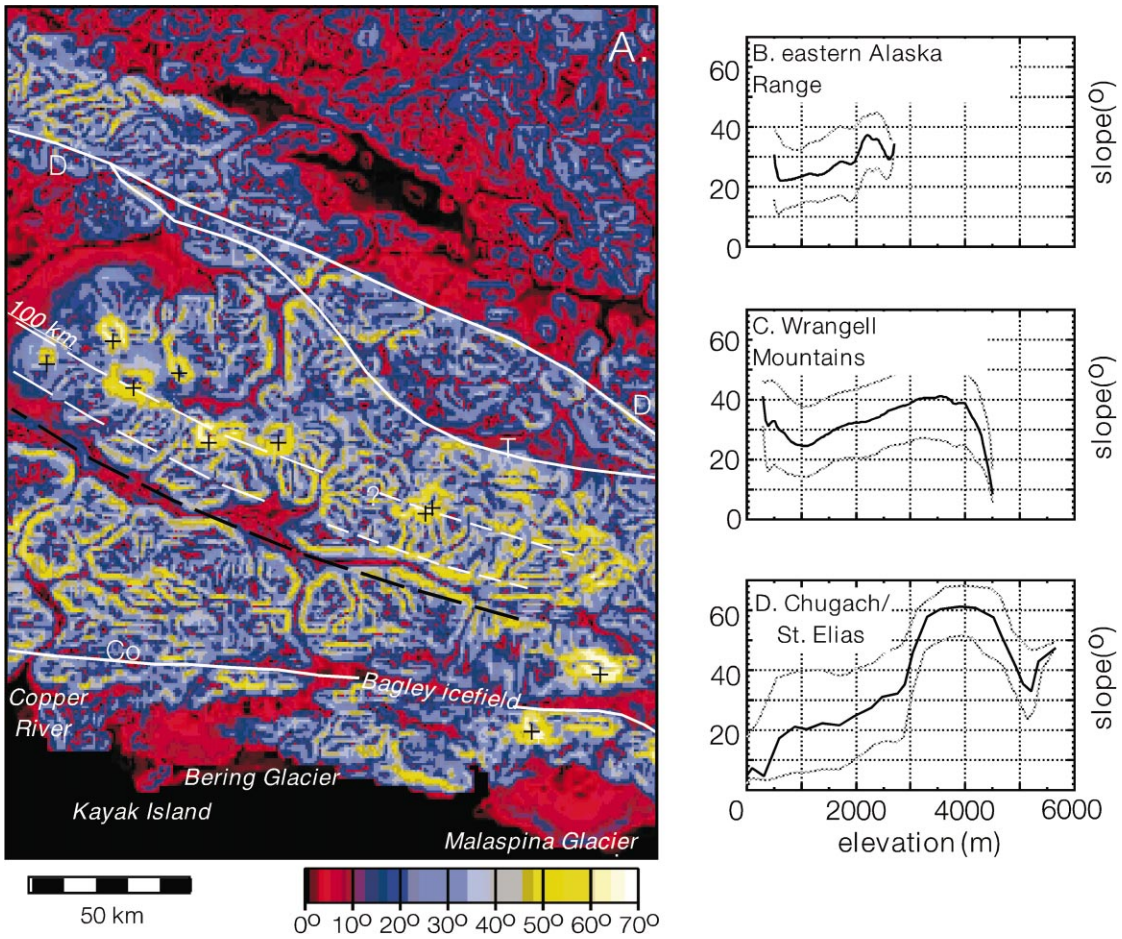

Fig. 6. Map of slope (a) and slope/altitude distribution for the eastern Alaska Range (b), Wrangell Mountains (c), and Chugach/St. Elias Range (d). The 25th, 50th (bold curve), and 75th percentiles of slope distribution are plotted. Note that the form of the curve for the Wrangell Mountains above 3500 m is influenced by the form of the stratovolcanoes. A slope minima coincides with the present range in elevation of the ELA in the Chugach/St. Elias where it is controlled in part by deglaciated glacial valley bottoms and in part by the surface of the Malaspina and Bering glaciers, the Bagley Ice field (the valley marked by the Contact fault (Fig. 3), and other glaciers within the range.

Range. On the low elevation end of the plateau, the Alaska Range differs from the Chugach/St. Elias in that it is characterized by higher slopes, $\sim 30^{\circ}$ in comparison to $< 10^{\circ}$, respectively. Much of the low altitude reaches of the Chugach/St. Elias Range are dominated by glacier upper surfaces (Fig. 6a), which appear as broad, low-relief, low altitude surfaces on the slope map, whereas the valley bottoms in the eastern Alaska Range tend to be narrow and characterized by high slope angles. The difference in form may reflect lack of glacial erosion or fluvial modification of formerly glaciated valleys in the eastern Alaska Range (Duncan et al., 1998). A significant fraction of the landscape (70%) in the Chugach/St. Elias Range (from 800 to 2800 m) has an average slope angle of 20 to 30° (compare Figs. 3d and 6d). Large slope angles are associated with valley walls and the regions around the high peaks.

Slope/altitude distribution in the Wrangell Mountains contrasts with that of the adjacent ranges (Fig. 6c). Whereas the lowest and highest elevations are characterized by high slope angles (up to 40°), slope angle changes smoothly with increasing altitude from a local minima at 1000 m. Each individual volcanic edifice in the Wrangell Mountains shows a similar slope distribution suggesting that their form dominates the signal in the slope angles above ~ 3000 m elevation (Figs. 3a and 6a). Like the other ranges, high slopes at low elevations occur on valley walls.

4. Modern ELA and topography

In this and the following section we focus specifically on the Chugach/St. Elias Range because its topography is a function of the interaction between climate, glaciers, and crustal deformation. Widespread coverage by glaciers today and a well-documented chronology of glacial fluctuations in the late Quaternary and Holocene (Tarr,

1909; Miller, 1961; Denton and Stuvier, 1966; Denton, 1974; Péwé, 1975; Denton and Karlén, 1977; Mann and Ugolini, 1985; Molnia, 1986; Calkin, 1988; Porter, 1989a; Hamilton, 1994), allow exploration of linkages between glacial erosion, glacier extent, and long-term denudation and topography.

In order to avoid confusion arising from various terms used to characterize the present altitudinal and spatial distribution of glaciers, several definitions are provided. Discussion focuses on the present orientation of the equilibrium line altitude (ELA), the position on a glacier where the net mass balance equals zero (i.e. accumulation = ablation (Paterson, 1994)), and its relationship with topographic trends. Snowline and glaciation thresholds are used below as proxies for the ELA. However, neither snowline nor glaciation threshold are strictly synonymous with the ELA. Snowline is the line on a glacier surface marking $>50\%$ surface cover by snow in the late summer and roughly coincides with the ELA (Péwé, 1975). Glaciation threshold is 'a critical minimum summit altitude which is necessary for a mountain to obtain (or maintain) a glacier' and is typically several hundred meters higher than the ELA (Østrem, 1972; Porter, 1977; Østrem et al., 1981).

Several methods have been used to characterize the regional distribution of glaciers (Péwé, 1975; Østrem et al., 1981; Mayo, 1986). Østrem et al. (1981) published a 1 : 2,000,000 map of glaciation threshold throughout southern Alaska. The elevation of threshold was established between the highest mountain without a glacier and the lowest mountain with glacier. A limitation of this method is that in area like the southern flank of the Chugach/St. Elias where glaciers extend to sea level, no peak below the present extent of the glaciers exists, glaciation level cannot be defined and the ELA cannot be approximated. Modern snowline across Alaska was mapped from the altitude of snowlines on glaciers in small, north-facing cirques (Péwé, 1975), Within the Chugach/St. Elias Range specifically, Mayo (1986) used US Geological Survey 1 : 63, 360 scale maps to determine the ELA position for the region between the Bering Glacier, Malaspina Glacier, and Bagley Ice field (Fig. 7). ELA estimates for individual glaciers were plotted and contoured. Although the method employed in this study is robust (ELA is indicated by the change from concave-downstream to concave-upstream in contour geometry), the analysis was based on maps published in 1959. Glaciers in the area have receded dramatically over the past century (Tarr, 1909; Tarr, 1914; Molnia, 1986; Porter, 1989a). Some uncertainty arises from the fact that this mapping is based on more elaborated glaciers and covers only the southern and eastern portions of the range. General consistency in altitude and trends of glaciation threshold, snowline, and ELA provides confidence that the ELA is characterized adequately, despite difference in scale and methodology.

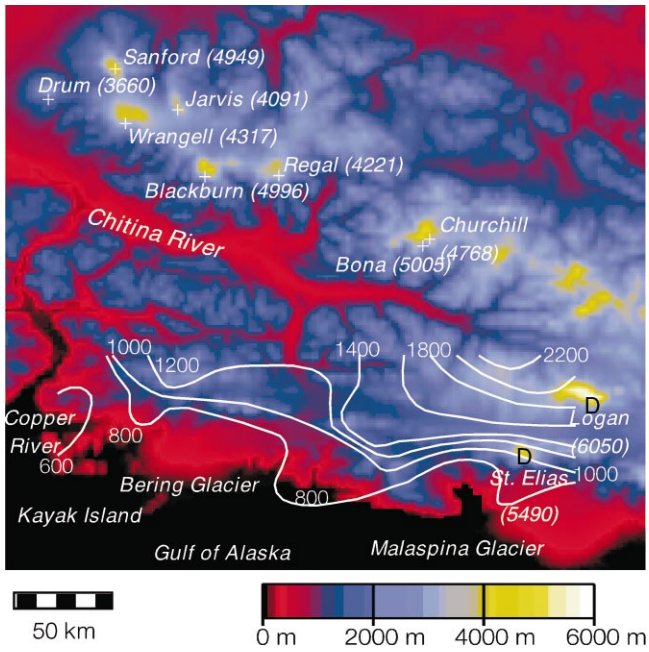

Fig. 7. Contours of the modern ELA (white lines) after Mayo (1986) superimposed on the DEM from the southern half of the study area. Contours are in meters above sea level. Note that the contours define an east-trending plane that climbs elevation at ~ 27 m/km to the north. Surface elevation and the ELA provide a visualization of the fact that $>50\%$ of the landscape lies at or above the ELA presently (Fig. 3d). Mt. St. Elias and Mt. Logan project more than 4 km above the ELA.

A 27 m/km rise in the ELA, from an elevation of <800 m near the coast to >2000 m west of Mt. Logan across the southern flank of the range, is indicated (Fig. 7). The ELA defines a complex surface that strikes west and faces both south and west (Figs. 7 and 8). Changes in the ELA, mean annual precipitation, and mean annual temperature correlate across the range (Fig. 8) (Péwé, 1975). Local topography affects the topology of the ELA in detail (Fig. 7). Landward cusps in the ELA occur just north of the Bering glacier in the vicinity of profile 5 (Fig. 3a), and at the Copper River valley (see also Fig. 11; Péwé, 1975). Both cusps coincide with significant embayments in the southern flank of the range. Topographic lows corresponding with these embayments likely facilitate landward penetration of storm systems, which would promote enhanced snowfall, and higher temperatures within the reentrants (Østrem, 1972; Péwé, 1975; Porter, 1975, 1977; Østrem et al., 1981). That the present ELA is low (~ 600 m) on the south arises from the combination of the high latitude of the range ($\sim 60^{\circ}$N) and maritime proximity (Andrews et al., 1970; Péwé, 1975; Porter, 1977, 1988; Østrem et al., 1981; Broecker and Denton, 1990).

Plotting the altitudinal range of the ELA on the hypsometric curve for the Chugach/St. Elias Range reveals that more than 50% of the landscape presently lies at or above the ELA (Fig. 3d). In detail, however, land surface

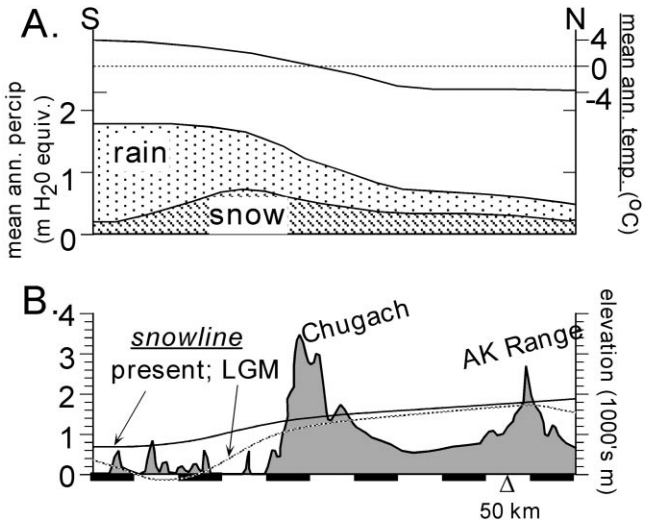

Fig. 8. Plot of (A) mean annual precipitation and annual temperature and (B) topography, present snowline, and last glacial maximum (LGM) snowline. Note the strong orographic effect of the Chugach/St. Elias Range on precipitation. Where topography has relatively little effect on precipitation and temperature on the south, the present snowline lies between 600 and 800 m above sea level. Modified from Péwé (1975).

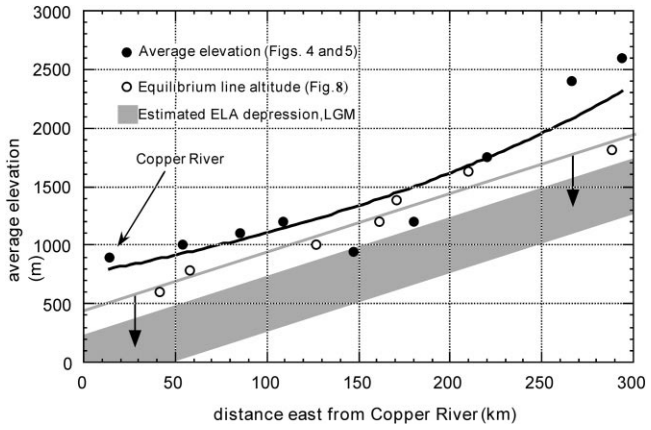

Fig. 9. Plot of along-strike variations in mean elevation within the Chugach/St. Elias Range. Individual data points are mean elevation values for profiles 1–8, from east to west, respectively (Figs. 3 and 4). Included is a ninth data point (on the west), for a profile not plotted in Fig. 4. A curve fit is plotted to emphasize an exponential decay in mean elevation from east to west, respectively. The present elevation of the ELA along the same west-to-east transect is plotted for the intersection of the transect with contours on the ELA (white dots), presented in Fig. 7 (Mayo, 1986). The shaded band denotes the likely range of ELA depression; estimates that range from ~200 m (Péwé, 1975), to ~1000 m (Porter, 1988) for the last glacial maximum, to ~500 m for average Quaternary climate (Porter, 1989b).

elevation in only slightly higher than the ELA surface (Fig. 9). Mean elevation is ~100–300 m higher than the ELA on average, with the exception of two areas. The north-trending topographic saddle in the central part of the range is an area where mean elevation lies below the ELA (profiles 5 and 4, 180 and 150 km, respectively, Figs. 3d and 9). In contrast, mean elevation is 600–800 m higher than the ELA in the east (profiles 1 and 2, 290 and 260 km, respectively, Figs. 3 and 9). Summit elevations of Mts. Logan and St. Elias are ~4000 m higher than the ELA.

Hypsometry provides a means for estimating the extent of changes in glacial coverage, or percent area influenced by ice, as a function of shifts of the ELA. Lowering of the ELA to that of a full glacial climate moves roughly ~75–95% of the landscape above the ELA, depending on the magnitude of ELA depression (Figs. 3d and 9) (Péwé, 1975; Porter, 1988, 1989b). That estimate is misleading, to a certain extent, because the magnitude of elevation shift varies significantly between the windward and leeward side of the range (Fig. 8). On the southern, windward flank of the range, a 75–95% change is reasonable given estimates of ELA lowering at the last glacial maximum (Péwé, 1975). Estimates of ELA lowering on the northern, leeward side of the range are significantly smaller (~100–200 m, Fig. 8; Péwé, 1975), although last glacial maximum terminus positions 75–250 km to the north of present termini of glaciers on the north flank of the range (Denton, 1974), imply that a 100–200 m lowering may be an underestimate. If ELA lowering is less on the northern flank, as expected for the leeward side of a rage (Porter, 1977; Porter et al., 1983), glacial extent on the north ought to be much less than on the south.

5. Implications for mean, orogen-scale 'glacial' erosion of climate change

Mean, orogen-scale 'glacial' erosion is a two-component system: (1) primary bedrock erosion along the ice-bedrock interface by glaciers and (2) erosion by other processes in areas peripheral to, but not in direct contact with, glacial ice. Quantifying the extent to which the land surface moves relative to the ELA provides a qualitative sense of the temporal variation in percent surface area covered by glaciers. Even though the percent change is not specified explicitly by such approximations, the estimates suggest that the locus of primary bedrock erosion by glaciers should oscillate in synchrony with altitudinal shifts of this plane due to climatic fluctuation (Fig. 10), if glacial erosion is a function of mass flux through the ELA (Andrews, 1972; Harbor, 1992). Moreover, the down-valley extent of glaciers on the windward and leeward flanks of the range during a given climatic state (i.e. full glacial), will vary as a function of orographically moderated differences in precipitation and temperature across the range (Figs. 8 and 10) (Østrem, 1972; Péwé, 1975; Porter, 1977; Østrem et al., 1981).

The glacial, interglacial, and mean position of the ELA thus define an across-strike and altitudinal band where

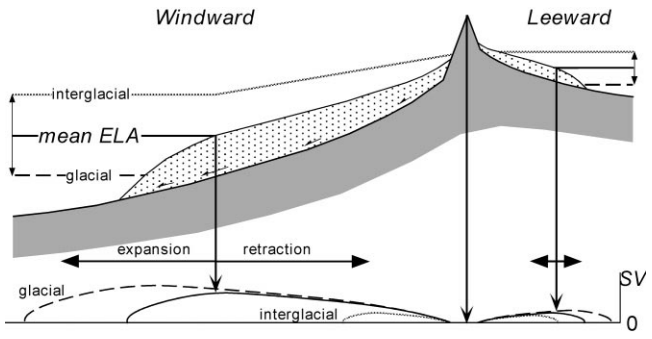

Fig. 10. Model illustrating the relationship between sliding velocity (SV and small arrows at the base of the windward glacier) and the ELA across an orogenic belt. An orographically induced rise in the ELA from the windward to the leeward side of the range leads to a higher mean ELA (solid back) line (see Figs. 7 and 8). Smaller amplitude fluctuations of the ELA between glacial (dashed line) and interglacial (gray line) is shown schematically (the leeward range in $\sim 33\%$ of the windward range, consistent with that of the Chugach/St. Elias). Assuming that bedrock erosion rate scales with basal sliding velocity (Hallet, 1979; Humphrey and Raymond, 1994), the model suggests concentration of erosion in a topographic band whose height is dictated by glacial/interglacial altitudinal limits to the ELA and whose width is a function of the concomitant glacial expansion/retraction in the landscape. The windward band width and height are likely to be greater than those of the leeward flank. Note that the range crest is defined by a topographic peak that corresponds spatially with a zone of low erosion rate by glaciers (arrow).

primary bedrock erosion by glaciers is focused, a band which, by definition, coincides with the maximum sliding velocity at a glacier's base (Fig. 10). On the windward, southern flank of the Chugach/St. Elias range specifically, the bandwidth is likely to be particularly wide because the ELA is at ~ 600 m and many of glaciers are at or near sea level (Mann, 1986; Molnia, 1986; Porter, 1989a). Tidewater glaciers are prone to large down-valley advances accompanying modest lowering of the ELA (Mercer, 1960). Significant increases in accumulation areas are predicted because of the low surface gradient of tidewater glaciers. Additionally, a lower calving rate per surface area decreases ablation rates at the terminus in the case of coalesced glaciers. Consequently, large increases in ablation zone area and concomitant down-valley advance are required to compensate for the combined changes in accumulation zone area and ablation rate (Mercer, 1960).

Primary bedrock erosion also occurs in ice marginal areas as a function of changes in the distribution of ice in the landscape. The magnitude of the landscape response to deglaciation in upper Taan Fjord (Fig. 11), suggests that a substantial component of the orogen-scale denudation is contributed by erosion in areas that are either periglacial or are ice-free only at glacial minima. Taan Fjord is one arm of Icy Bay created by the retreat of the Tyndall glacier over the past 40 years, a retreat beginning at the turn of the century when the Icy Bay glacier system extended to the mouth of the bay, flush with the Pacific coastline (Porter, 1989a). Tyndall glacier lies at the foot of Mt. St. Elias (Fig. 3a). Aerial photographs and new mapping document that glacial retreat between 1983 and 1996 was accompanied by a mountain-scale landslide failure of the fjord wall, 10's-of-meter scale incision of bedrock gorges by proglacial streams, remobilization of colluvial and fluvial deposits more than 300 m thick and graded to the former margin of the glacier, and construction of large fan-delta systems where tributary valley debouch into the fjord (Fig. 11a, b).

The landslide covers an area of $\sim 0.4\,km^2$, extends from sea level up to 600 m, has a surface length of 1.4 km, an average slope of 26° and a $\sim 60°$-dipping, 200 m-high head scarp (Fig. 11c). Bedrock structure is cross-cut by the head scarp and strikes subparallel to the fjord wall (Fig. 11b). Scarps within the landslide are antithetic to the head scarp, vary in dip from 50 to 70°, and have separations up to 30 m. Net down-dip displacement on the base of the landslide is ~ 300–400 m (8–16% extension) derived from the sum of displacements on each scarp. Surface height of the Tyndall glacier in 1983 was ~ 470 m, established from trimline elevation on the valley wall and field calibration of the 1983 aerial photographs. Assuming a 35° initial valley-wall slope angle (direct measurement and surveying suggest 35° is representative), wall length increased rapidly from ~ 700 m in 1983 to 1780 m on deglaciation; a slope length increase of 150%. Smaller deep-seated landslides in the Coal and Daisy glacial valleys also disrupt recently abandoned trimlines (Fig. 11a). Plotting the ridge minus trimline height against trimline minus ice (or valley-bottom) elevation for these landslides suggest that valley wall length changes due to reduction of ice elevation on the order of 50–100% may have promoted these failures (Fig. 11d). A mechanism of bedrock landsliding whereby valley walls are destabilized following ice retreat moving the landscape towards failure by deep-seated landsliding is suggested. This pulse of sedimentation has been promoted by the change from glacier-filled to glacier-absent conditions (Fig. 12). Similar high sedimentation rates have been inferred for Icy Bay and other Alaskan fjords (Powell, 1983; Porter, 1989a; Hallet et al., 1996).

An approximation of percent changes in ice coverage in Taan Fjord can be made by integrating terminus positions at the turn of the century and at the last glacial maximum with a model that provides a reasonable approximation of glacier surface elevation with distance from the terminus (Paterson, 1994) (Fig. 13). Historic records and photographs demonstrate that Icy Bay was ice-filled at the turn of the century (Porter, 1989a). Although the extent to which glaciers in coastal Alaska covered the continental shelf is not well-constrained, a number of lines of evidence suggest they extended more 60 km southward from the present coast to the edge of the continental shelf (Molnia, 1986; Hamilton, 1994).

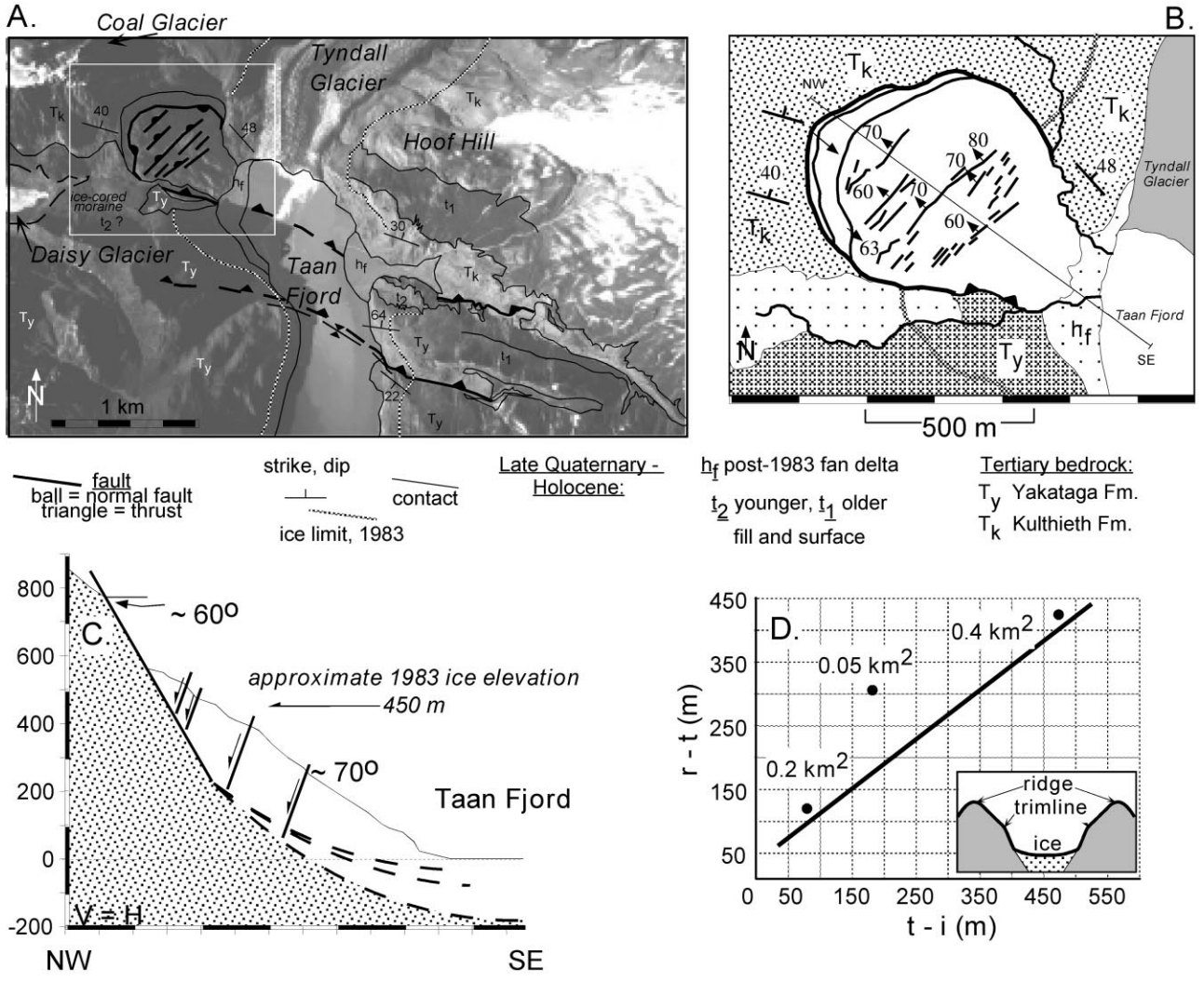

Fig. 11. Landscape effects in the upper reach of Taan Fjord following retreat of the Tyndall Glacier to its present position by 1996 A.D. (A) Air photo map with geology overlay of the terminus region of the Tyndall Glacier depicting a large (0.4 km^2, 1.5 km wide, 600 m high) landslide on the west side of Taan Fjord and a deeply dissected sequence of ice-marginal colluvial and fluvial deposits on the east side. Air photos from 1983 do not reveal the presence of the landslide and indicate only moderate dissection of the ice-marginal deposits. The 1983 ice elevation, marked today by a pronounced trimline, is marked and lies at $\sim$ 450 m above sea level. Note that two bedrock thrust faults do not cut the surficial deposits. A white box indicates the location of the detailed map of the landslide in (B). The strike of the head scarp parallels the valley wall and cross-cuts bedrock structure. (C) A cross-section illustrates the 60° dip and $>$ 200 m separation across the head scarp and the $>$ 70° dip of a suite of antithetic scarps. Total down-dip displacement of the landslide is uncertain due to an unknown depth to the bottom of Taan Fjord. (D) A plot of ridge-trimline height versus trimline-ice (or valley bottom) height suggests that slope lengthening on the order of 50–100% may explain the occurrence of this and other bedrock landslides as the result of loss of valley-wall support by ice.

Because bathymetry data are discontinuous for Icy Bay, the depth of Taan Fjord is unknown at present and thus represents an error of as much as several hundred meters on estimates of absolute elevation of the Tyndall glacier.

Projection of the reconstructed glacier-top for the 1900 AD terminus and assuming $-$ 200 m depth to the fjord is consistent with trimline elevations along the fjord walls calibrated in the field. It should be emphasized that the principal purpose of this model (Fig. 13) is to make approximations of the percent change in surface coverage by glaciers of the landscape. The west wall has roughly twice the relief relative to sea level of the east wall, which serves to emphasize the importance of local relief on reconstructions of ice coverage. Between 43 (west) and 64% (east) of the valley wall would be ice covered for the 1900 AD projection of the surface back into the landscape. Ice would over-top the east wall and cover more than 80% of the west wall at the last glacial maximum.

Sediment delivered to the fjord on deglaciation presumably would be removed from the orogen by a readvance to the 1900 AD position. Stratigraphic data suggest that such readvances take $\sim$ 300–500 years, at least over the past 2000 years (Porter, 1989a). Significant advances of the Icy Bay glacier network on relatively short time

scales is consistent with recent theoretical models that indicate that large glaciers have short response times to changes in mass balance (i.e. climate change) (Bahr et al., 1998; Pfeffer et al., 1998). Moreover, considerable expansion of a tidewater glacier network accompanying small climate shifts is predicted when the ELA is close to sea level (Mercer, 1960). If changes in valley wall-support create a threshold for bedrock landsliding (Fig. 11d), modest century-scale glacial fluctuations might cause concomitant changes in the frequency and magnitude of bedrock landslides. However, the magnitude of valley deepening and wall over-steepening during the period of each advance/retreat cycle likely dictates whether advance/retreat frequency and landslide frequency are directly or inversely related (K. Whipple, 1999, pers. comm.).

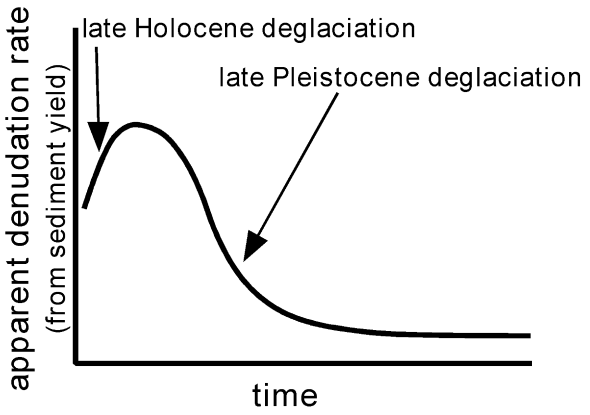

Fig. 12. Model relating a disequilibrium pulse in sedimentation accompanying deglaciation (modified from Church and Ryder, 1972). Time is not scaled, Taan fjord represents < 10 year since ice retreat (late Holocene) whereas the late Pleistocene line represents data from southwestern British Columbia (Church and Slaymaker, 1989), and represents 1000 s of years following deglaciation.

6. Linkages between uplift, erosion, climate, and topography

Active orogenic topography is dictated by the magnitude of tectonic flux of rock from below relative to the erosive flux by the geomorphic systems operating from above. Because geomorphic systems are forced by both climate and tectonics (Bull, 1991; Whipple and Tucker, 1999), two classes of potential feedbacks merit consideration. First, how does topography at the orogen scale compare with uplift and denudation rates (i.e. across the Chugach/St. Elias range)? If topographic change is modulated by competition between rates of uplift and erosion, it becomes important to place independent constraints on the rates and patterns of uplift and denudation. Coupling and feedback between uplift and erosion implies that they ought to correlate (Willett et al., 1993; Koons, 1994, 1995; Beaumont et al., 1996). Second, do

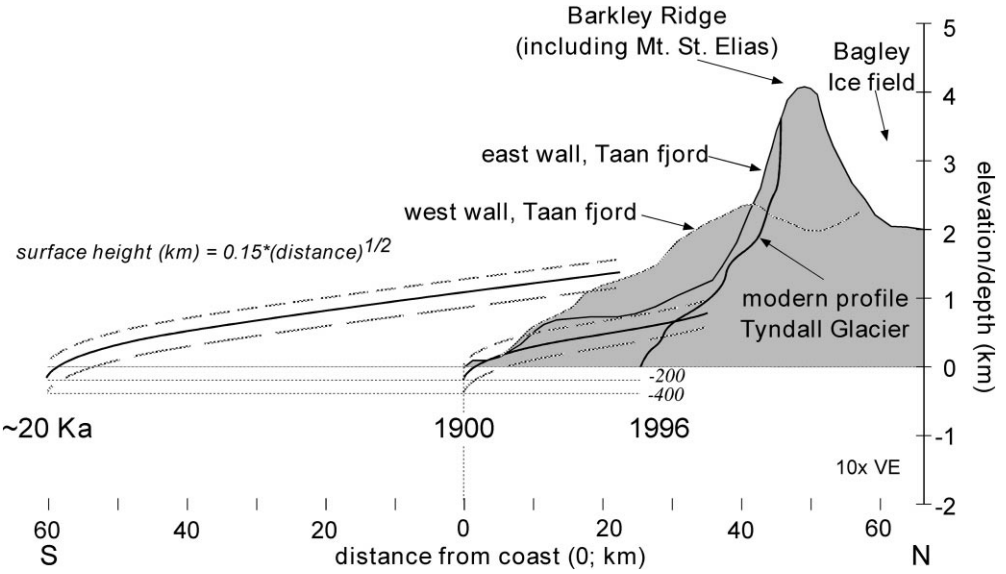

Fig. 13. Topographic profiles of the east and west margins of Taan Fjord and the surface profile of the Tyndall glaciers. Model surface elevations of the Tyndall Glacier at its 1990 AD and last glacial maximum position ($\sim$ 20 ka) are based on an equation relating surface height to distance from terminus (Paterson, 1994). Uncertainty arises from the unknown depth of Taan Fjord, although the surface projection for the 1900 AD position and $-$ 200 m depth is consistent with trimline elevations along Taan Fjord. Note that between 25 and 85% of valley walls would be ice covered for the 1900 AD projection, depending on local relief, and that more than 80% would be ice covered at 20 ka regardless of local relief. Barkely Ridge is an east-treading ridge of high peaks, including Mt. St. Elias, that lies between the Chugach/St. Elias and Contact faults (Fig. 3a). The surface height model is used to provide order-of magnitude estimates of glacial coverage of the landscape. Because the model is most appropriate for an ice sheet lying on a flat bedrock surface, it may not apply strictly to alpine valley/tidewater glacier systems.

specific characteristics in the form of landscape (i.e. mean elevation, slope, hypsometry, relief), reflect feedback between uplift, topography, and climate? That mean fluvial topography scales with uplift rate is suggested by models that show close coupling between drainage network geometry and uplift rate (Tucker and Bras, 1998; Whipple et al., 1999; Whipple and Tucker, 1999). However, connections between glacial drainage network geometry and uplift rate have not been explored quantitatively.

Fault displacement rates are poorly constrained within the study area. Geodetically determined horizontal rates are consistent with plate convergence rates (DeMets et al., 1994; Sauber et al., 1997), but the data are not sufficiently dense to discriminate velocity gradients across individual faults (Sauber et al., 1999). Because the uplift component of the geodetic data represents interseismic elastic strain accumulation, the relationship of uplift rates derived from geodetic data to long-term average rates is uncertain. Roughly 1 m of coseismic uplift in the region of Icy Bay occurred during a 1899 earthquake sequence; an additional ~ 1 m is inferred to have accumulated elastically in the subsequent 100 years (Tarr and Martin, 1912; Sauber et al., 1999). Because of these uncertainties, order-of-magnitude estimates of uplift rate across the Chugach/St. Elias range were made via a simple model combining horizontal rates and dip of the individual major faults (Fig. 14a and b).

Dip of the major faults, including (1) the plate boundary fault separating the Yakutat terrane upper plate from the Pacific lower plate, (2) the deformation front within the Yakutat terrane, and (3) the Chugach/St. Elias thrust, increases from south to north (Fig. 14a). Models and some data suggest that horizontal displacement rates increase systematically between the individual major faults from south to north, respectively (Fig. 14a) (Plafker et al., 1994a; Lundgren et al., 1995; Bird, 1996), although deformation appears to be shifting south with time (Plafker, 1987). Local uplift rate is derived from the product of the horizontal rate and the tangent of the fault angle. Uplift rate determined in this manner is sensitive to both fault dip and horizontal rate and varies from ~ 1 mm/yr on the south to 10 mm/yr or greater on the north (Fig. 14b). Implicit in this model is the assumption that the partitioning of horizontal rate predicted by plate deformation models approximates the 'true' partitioning across the major faults. Moreover, partitioning of horizontal displacement on minor faults not considered in the model would modify an uplift-rate pattern based on the major structures alone.

Existing data give conflicting views of erosion and exhumation rates regionally. Erosion rates inferred from Alaskan glacier sediment-yield data range from ~ 7 to 50 mm/yr (Hallet et al., 1996). The sediment-yield data are interpreted to reflect primary bedrock erosion rates, although it seems probable that part of the signal within these data reflects a modern disequilibrium sediment

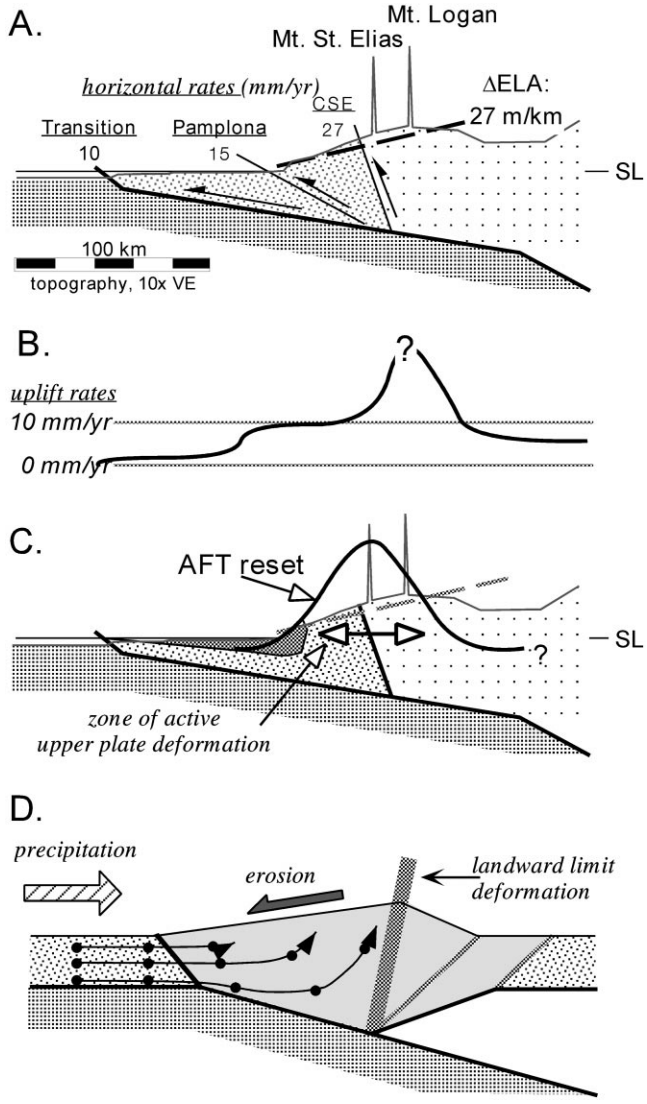

Fig. 14. Schematic north–south cross-section across the plate boundary and Chugach/St. Elias Range at the longitude of Icy Bay (Fig. 3a). The upper plate includes the Yakutat terrane (Y; coarse stipple, dark gray in (C) represents upper Tertiary rocks of the Yakataga Formation), overthrust by North America (NA, open stipple) on the Chugach/St. Elias thrust (CSE). Separated by the plate boundary megathrust, the Pacific Plate (P, light gray pattern) underlies both upper plate blocks. Surface area/altitude distributions are constrained by the hypsometry such that the area above ~ 3500 m occupies less than 5% of the cross-sectional area. ELA orientation is based on Fig. 7. (A) Cross-section incorporating the principal tectonic elements within the Chugach/St. Elias Range. Horizontal velocity for the Transition fault (T) is from Plafker et al. (1994a); for the CSE is from the model results of Lundgren et al. (1995) and Bird (1996), and for the Pamplona thrust (P), which separates the unreformed offshore portion from the deformed onshore portion of the Yakutat terrane, is the residual of the ~ 42 mm/yr convergence of Y-NA (Plafker et al., 1994a). (B) Smoothed uplift rate curve derived from the product of the horizontal rate and the tangent of the fault angle. (C) Exhumation window suggested by the altitudinal and across-strike position of Pliocene and younger apatite fission-track (AFT) cooling ages (data from O'Sullivan and Currie, 1996; O'Sullivan et al., 1997). (D) Coupled erosion deformation model where the dominant precipitation is from the same direction as the flux of rocks into the orogen (modified from Willett et al., 1993). Coarse stipple pattern are undeformed rocks, light gray represents deformed rocks within the orogen, dark, thick lines are active shears, shaded, thick lines are inactive shears, and dots and curved lines with arrows represent particle trajectories.

yield (Fig. 12). If these rates do approximate primary bedrock erosion rates, they are of the same order of magnitude as the inferred rock uplift rates (Fig. 14b). Cooling ages from apatite fission-track data are inferred to constrain exhumation rate to $\sim$ 1.5 mm/yr regionally (O'Sullivan et al., 1997). It is difficult to evaluate the veracity of this rate because a majority of the samples on which it is based are randomly distributed along a 90 km-long belt and a small elevation range ($\sim$ 1500 m) along the eastern boundary of the Yakutat terrane.

Nevertheless, these fission-track data, when combined with apatite fission-track cooling ages from a vertical relief section on Mt. Logan (O'Sullivan and Currie, 1996), are suggestive of the form of exhumation across the range at the longitude of Mts. St. Elias and Logan (Fig. 14c). Reset Pliocene ages are revealed by samples below 2500 m on Mt. Logan (O'Sullivan and Currie, 1996), a sample from $\sim$ 3300 m on Mt. St. Elias (O'Sullivan et al., 1997), and samples from the footwall of the Chugach/St. Elias thrust in Yakutat Bay (Fig. 2) (O'Sullivan et al., 1997). A window of exhumation, with a peak centered on Mt. St. Elias, is implied by the distribution of Pliocene and younger resent apatite fission track ages. This peak coincides with the oldest rocks exposed at the surface within the Yakutat terrane (Fig. 14c) (Plafker, 1987), the locus of historic seismicity (Tarr and Martin, 1912; Eastabrook et al., 1992; Plafker et al., 1994a; Sauber et al., 1999), and the inferred peak in uplift rate (Fig. 14b).

The pattern of uplift rate, exhumation, active upper plate deformation, and age of rocks exposed at the surface bears striking similarity to those predicted by a coupled erosion/deformation model (Fig. 14d) (Willett et al., 1993). Similarities include: (1) the dominant moisture source is in the same direction as the flux of rock into the orogen (Fig. 8); (2) a one-sided orogen with a landward limit to recent deformation that coincides roughly with the crest of the orogen (Fig. 14a); (3) a 'dry' leeward flank characterized by a low erosion rate (in the case of the Chugach/St. Elias the leeward flank is characterized by lower mean annual temperature, precipitation, and a higher mean ELA; Figs. 8 and 10); (4) a gradient from shallow to deep in depth of rocks exposed at the surface (Fig. 14c); and (5) localization of the deepest rocks, those likely to have young cooling ages, adjacent to the landward deformation limit. Differences such as the narrow aperture of zone of rock uplift and narrow topographic width in the Chugach/St. Elias are explained by the fact that the deformed zone is relatively narrow at the longitude of Mts. St. Elias and Logan, that part of the deformation occurs offshore, and that the width of the shallow portion of the down-going plate changes systematically along strike from east to west.

These parallels support speculation that (1) mean erosion rates match rock influx/uplift rate and (2) the erosion acts to modulate the locus of uplift in the Chugach/St. Elias range. Positive feedback between erosion and uplift is manifest in the topography; mean elevation reaches a maximum within the high uplift/exhumation-rate window (compare Figs. 4, 5 and 14). The distribution of high peaks also coincides with the window and is not random. Both Mt. St. Elias and Mt. Logan are located on east–west trending ridges bounded by massive glacier systems and icefields (Fig. 3). Mt. St. Elias lies on a 130 km-long east–west trending ridge bound by the south-flowing Yahtse/Tyndall glacier systems on the south and the west- and east-flowing Bagley/Seaward ice fields ($\sim$ 1800 m elevation) on the north. Mt. Logan lies on a 120 km-long east–west treading ridge bound by the Bagley/Seaward ice fields on the south and a blanket of north-flowing, coalesced valley glaciers and ice fields on the north. Thus, the high peaks lie in a unique position where glacial erosion rates must be essentially zero (Compare Figs. 10 and 13). The development and residence time of peaks above the mean landscape, in the face of uniform uplift rates (at $\sim$ 20 km wavelength across the ridges), likely reflects a lower (?) erosion rate set by the frequency of large bedrock landslides and rock strength (Schmidt and Montgomery, 1995; Brozovic et al., 1997).

7. Discussion

Is it possible to argue that the ELA, hence climate, sets a limit to the topography of southern Alaska as has been suggested for the northwest Himalaya? Substantial evidence suggests that topography controls the ELA (Andrews et al., 1970; Østrem, 1972; Porter, 1977; Østrem et al., 1981; Porter et al., 1983). Correlation of mean elevation, slope, hypsometry, and the ELA, a correlation argued to suggest a climatic limit to topography in the northwest Himalaya (Brozovic et al., 1997), is a fundamental prediction of a topographic control on the ELA. A climatic limit in the northwest Himalaya is credible given that structural trends are nearly orthogonal to climatic and topographic trends. In contrast, structural, climatic, and topographic trends are parallel in the Chugach/St. Elias range (compare Figs. 3a, 5 and 7). Modern gradients in temperature and precipitation across the range are interpreted to indicate a topographic control on climate across the range (Fig. 8) (Péwé, 1975). Thus, a positive feedback likely exists between rock uplift in the core of the range and orographically modulated precipitation and temperature distributions, because the core is the site of high mean elevation and mountain peak formation (Fig. 14). Peak formation and maintenance is important in that the peaks likely form barriers to northward flow of storm cells off the Pacific Ocean, which enhances snowfall in particular. Such a sequence implies larger mass fluxes (and higher sliding velocities; Andrews,

1972; Hallet, 1979; Humphrey and Raymond, 1994), for the system of glaciers on the southern, windward side of the Chugach/St. Elias Range than on the north side.

Whereas the postulated positive feedback loop between uplift, erosion, topography, and climate is intriguing, it does not address satisfactorily the question of climatic control on orogenic topography. For example, what places the upper bound on mean elevation? In fluvial landscapes, mean elevation is controlled by drainage basin spacing, relief, and elevation of the drainage outlets, which are likely set by uplift rate (Densmore et al., 1998; Tucker and Bras, 1998; Whipple and Tucker, 1999). Although quantitative relationships between glacial drainage basin geometry, glacial erosion, and active uplift have not been developed, potential insight is gained by consideration of the connection between glaciation threshold and latitude (Østrem, 1972; Porter, 1977, 1988; Østrem et al., 1981; Porter et al., 1983; Broecker and Denton, 1990). High latitudes are characterized by lower glaciation thresholds than low latitudes. Thus, if the ELA is a proxy for the altitude range where erosion by glaciers reaches a maximum, it follows that the efficiency of glacier erosion would, all else being equal, lie at a lower altitude at high latitude than at low latitude.

Interestingly, Fig. 8b describes the altitudinal range of the ELA, given the climate of 60°N and the absence of significant topography (south end, Fig. 8b), and suggests potential consequences of active uplift at this latitude for ELA and mean topography. The interglacial and glacial snowlines in the Chugach range are higher ($\sim$ 400 and 800 m, respectively), and compressed relative to those in the south (Fig. 8b) (Péwé, 1975). This pattern may reflect the consequences for the ELA due to active uplift. Active uplift pushes the ELA to higher elevations than are anticipated for a given latitude. Creation and amplification of topography creates an orographic effect on local climate, which is expected to lower the ELA, as a function of the enhanced precipitation (if it is dominated by snowfall), in particular (Østrem, 1972; Porter, 1977; Østrem et al., 1981). Therefore, the ELA in a glaciated active orogenic belt is determined by latitude first (because of its control on the glacial/interglacial altitudinal range); departure from this altitudinal range reflects the competition between the tendency to raise the ELA due to uplift and the tendency to lower the ELA as a function of enhanced precipitation. An upper altitudinal limit to the ELA, for a given latitude, is hinted at by this competition. If glacial erosion rate scales with sliding velocity and sliding velocity reaches a maximum at the ELA (Andrews, 1972; Hallet, 1979; Humphrey and Raymond, 1994; Paterson, 1994), mean elevation may be coupled to the ELA and dependent, in part, on the altitudinal range of the ELA at a given latitude.

Variation in glacier extent as a function of climatic oscillation probably also plays a significant role in the feedback. Roughly equal amounts of time over the last 800 kyr are characterized by glacial and interglacial climates (Imbrie et al., 1984) (Fig. 1). Because the glacial system within Icy Bay has apparently fluctuated on 300–500 yr time scales in the late Holocene between the present coverage to that at the turn of the century (Porter, 1989a), transitions for full glacial to full interglacial likely are marked by high-frequency oscillations of ice coverage in the landscape and concomitant changes in erosional mode. Climatic models that imply a conversion of glaciers from warm-based to cold-based at the last glacial maximum (Hostetler and Clark, 1997), raise the complicating possibility that erosion rates are at their lowest at glacial maxima (due to lower sliding velocities; Paterson, 1994). A key implication for the long-term erosion of glacial-dominated orogens is set by climatic fluctuations, on frequencies ranging from 10^2 to 10^{4-5} yr. That control dictates the pace of bedrock erosion and sediment production by individual processes, the temporal variation of which is not well constrained.

8. Conclusions

1. Three discrete topographic domains are recognized from south to north, respectively: (1) the Chugach/St. Elias Range; (2) the Wrangell Mountains; and (3) the eastern Alaska Range.

   (a) The Chugach/St. Elias Range extends from the coast to the Chitina-Copper River valley and includes the two highest peaks in the study area, Mt. St. Elias (5490 m) and Mt. Logan (6050 m). Altitude in the Chugach/St. Elias Range is bimodally distributed with nearly equal amounts of area at 300 and 1200 m, a distribution that reflects, in part, the surface elevations of the extensive ice fields and glaciers and unoccupied glacial valleys. Mean elevation ($\sim$ 1225 m) is low in comparison with the elevation of highest peaks. More than 90% of the land area lies in an altitudinal band between 300 and 2200 m above sea level; the surface area above 3200 m occupies less than 2% of the landscape. Mean elevation decays exponentially from $\sim$ 2500 to $\sim$ 1100 m in less than 100 km west of Mts. Logan and St. Elias. Relief changes from east to west as well, from $\geqslant$ 2100 to $\leqslant$ 600–800 m, respectively.

   (b) A prominent series of stratovolcanoes ($\sim$ 4000–5000 m summits) dominates the topography of the northwest-treading Wrangell Mountains. Mean elevation (1670) is only slightly higher than the modal elevation (1500 m). Hypsometry is left-skewed due to the high elevations of the volcanic edifices. The volcanoes appear to have developed on a landscape with an initial elevation of $\sim$ 1800–2500 m regionally. Relief is relatively constant along strike.

   (c) The eastern Alaska Range is topographically subdued when compared with the Wrangell and

Chugach/St. Elias domains to the south. Altitude is normally distributed about the mean elevation, although the modal elevation (1100 m) is slightly lower than the mean elevation (1214 m). More than 30% of the area has elevations between 1100 and 1300 m. Peak elevations exceed 2600 m, yet these peaks occupy $\leqslant 1\%$ of the surface area. As a distinct topographic entity, the eastern Alaska Range maintains about the same height (~ 1000 m) and relief (< 600 m) across the study area.

2. Slope/altitude curves for the Chugach/St. Elias and eastern Alaska Range are similar. Both are characterized by central plateaus in slope bound by a step to substantially higher slope angles at higher elevations (from 20–30° to $\sim 60°$ at 3000 m in the Chugach/St. Elias Range and from 22–28° to $\sim 40°$ at 2000 m in the eastern Alaska Range). A significant fraction of the landscape (70%) in the Chugach/St. Elias Range (from 800 to 2800 m) has an average slope angle of 20–30°. At low elevations the eastern Alaska Range is characterized by $\sim 30°$ slopes, whereas low-altitude slopes in the Chugach/St. Elias are $< 10°$. Much of the low altitude portions of the Chugach/St. Elias Range are dominated by glacier upper surfaces that appear as broad, low-relief, low altitude surfaces. The valley bottoms in the eastern Alaska Range tend to narrow and characterized by high slope angles that reflects lack of glacial erosion or fluvial modification of formerly glaciated valleys. Slope/altitude distribution in the Wrangell Mountains is dominated by the form of the volcanic edifices.
3. A 27 m/km northward rise, from an elevation of < 800 m near the coast to > 2000 m west of Mt. Logan, characterizes the equilibrium line altitude (ELA) in the Chugach/St. Elias Range (Mayo, 1986). Surface elevation is only slightly higher, on average, than the west-striking, south-facing plane defined by the ELA regionally. Mean elevation corresponds with the ELA in the Chugach/St. Elias Range and more than 50% of the landscape lies at or above the ELA presently. Because the area above 3000 m represents $< 2\%$ of the surface area, the summits of Mts. Logan and St. Elias project like needles nearly 4000 m above the plane of the ELA. Between ~ 40 and 60% of valley wall would be ice converged given the extent of glaciers at the turn of the century. Eighty percent or more of the valley walls would have been covered at the last glacial maximum.
4. Net, range-scale erosion of 'glaciated' orogens is the sum of (1) primary bedrock erosion by glaciers and (2) erosion in areas of the landscape that are ice-marginal and are deglaciated at glacial minima. The later portions of the landscape are sensitive to changes in ice height and distribution. Ice height and distribution controls erosional processes in ice-free areas, processes such as deep-seated bedrock landsliding, fluvial incision of glacial valley bottoms, and remobilization of colluvial and fluvial deposits graded to the former glacier margins. The relative importance of glacial and other erosional processes in the net denudation per unit area of an orogen varies as a function of climate change operating on 10^2–10^5 time scales.
5. Topographic wavelength related to the width of the shallowly dipping segment of the plate interface and the spacing and geometry of major upper plate structures. Width and structural spacing increase from east to west. Topographic amplitude is controlled by the competition between uplift and primary bedrock erosion at the base of glaciers and in area peripheral to, but sensitive to, the height and extent of glaciers in the landscape. The mean distribution of glaciers is dictated by the maritime setting of the Chugach/St. Elias range and the 60° latitude. Differences in the mean distribution of glaciers between the southern, windward and northern, leeward flanks of the range imply larger erosion rates over a larger fraction of the orogenic surface on the south flank. Uplift apparently increases the ELA whereas raising topography creates an orographic effect on precipitation and temperature tends to lower the ELA. A positive feedback between erosion on the windward flank is postulated, in which erosion focusing of active deformation and rock uplift on the windward flank of the range. Thus, mean topography reflects the combined influences of latitude and feedback between mountain building due to uplift and concomitant orographic effects on climate and erosional patterns.

Acknowledgements

This research was supported by NASA's Dynamics of the Solid Earth Topography and Surface Change program. AJM was supported by a postdoctoral fellowship from the Division of Geological and Planetary Sciences, California Institute of Technology. Doug Burbank, Nick Brozovic, and Peter Clark are thanked for discussions. Kelin Whipple and an anonymous reviewer are thanked for insightful and challenging reviews that provoked a reappraisal of our interpretation and that helped to improve substainally the focus and analysis presented herein. Danny Rosenkrans and other members of the Wrangell-St. Elias Park service are thanked for their invaluable help and cooperation.

References

Andrews, J.T., 1972. Glacier power, mass balances, velocities, and erosion potential. Zeitschrift für Geomorphologie 13, 1–17.

Andrews, J.T., Barry, R.G., Drapier, L., 1970. An inventory of the present and past glacerization of Home Bay and Okoa Bay, east Baffin Island, N.W.T., Canada, and some climatic and paleoclimatic considerations. Journal of Glaciology 9 (57), 337–362.

Bahr, D.B., Pfeffer, W.T., Sassolas, C., Meier, M.F., 1998. Response time of glaciers as a function of size and mass balance: 1. Theory. Journal of Geophysical Research 103 (B5), 9777–9782.

Beaumont, C., Fullsack, P., Hamilton, J., 1992. Erosional control of active compressional systems. In: McClay, K.R. (Ed.), Thrust Tectonics. Chapmann & Hall, New York, pp. 1–18.

Beaumont, C., Kamp, P.J.J., Hamilton, J., Fullsack, P., 1996. The continental collision zone, South Island, New Zealand: comparison of geodynamical models and observations. Journal of Geophysical Research 101, 3333–3359.

Bird, P., 1996. Computer simulations of Alaskan neotectonics. Tectonics 15 (2), 225–236.

Broecker, W.S., Denton, G.H., 1990. The role of ocean–atmosphere reorganizations in glacial cycles. Quaternary Science Reviews 9, 305–341.

Brozovic, N., Burbank, D.W., Meigs, A.J., 1997. Climatic limits on landscape development in the northwestern Himalaya. Science 276, 571–574.

Bruns, T.R., Carlson, P.R., 1987. Geology and petroleum potential of the southeast Alaska continental margin. In: Scholl, D.W., Grantz, A., Vedder, J.G. (Eds.), Geology and Petroleum Potential of the Continental Margin of Western North America and Adjacent Ocean Basins-Beaufort Sea to Baja California. Earth Science Series, Houston, TX, pp. 269–282.

Bull, W.B., 1991. Geomorphic Response to Climate Change. Oxford University Press, New York, 326 pp.

Burbank, D.W., Leland, J., Fielding, E., Anderson, R.S., Brozovic, N., Reid, M., Duncan, C., 1996. Bedrock incision, rock uplift and threshold hillslopes in the northwestern Himalayas. Nature 379, 505–510.

Calkin, P., 1988. Holocene glaciation of Alaska (and adjoining Yukon Territory. Canada. Quaternary Science Reviews 7, 159–184.

Church, M., Ryder, J.M., 1972. Paraglacial sedimentation: a consideration of fluvial processes conditioned by glaciation. Geological Society of America Bulletin 83, 3059–3072.

Church, M., Slaymaker, O., 1989. Disequilibrium of Holocene sediment yield in glaciated British Columbia. Nature 337, 452–454.

DeMets, C., Gordon, R.G., Argus, D., Stein, S., 1994. Effect of recent revisions to the geomagnetic reversal time scale on estimates of current plate motions. Geophysical Research Letters 21, 2191–2194.

Densmore, A.L., Ellis, M.A., Anderson, R.S., 1998. Landsliding and the evolution of normal-fault-bounded mountain fronts. Journal of Geophysical Research 103 (B7), 15203–15219.

Denton, G.H., 1974. Quaternary glaciations of the White River valley, Alaska, with a regional synthesis for the northern St. Elias Mountains, Alaska and Yukon Territory. Geological Society of America Bulletin 85, 871–892.

Denton, G.H., Karlén, W., 1977. Holocene Glacial and tree-line variations in the White River valley and Skolai pass. Alaska and Yukon Territory. Quaternary Research 7, 63–111.

Denton, G.H., Stuvier, M., 1966. Neoglacial chronology, northeastern St. Elias Mountains, Canada. American Journal of Science 264, 577–599.

Duncan, C.C., Klein, A.J., Masek, J.G., Isacks, B.L., 1998. Comparison of Late Pleistocene and modern glacier extents in central Nepal based on digital elevation data and satellite imagery. Quaternary Research 49, 241–254.

Eastabrook, C.H., Nabelek, J.L., Lerner-Lam, 1992. Tectonic model of the Pacific–North American plate boundary in the Gulf of Alaska from broadband analysis of the 1979. St. Elias, Alaska earthquake and its aftershocks. Journal of Geophysical Research 97, 6587–6612.

Eyles, C., Lagoe, M., 1998. Slump-generated megachannels in the Pliocene–Pleistocene glaciomarine Yakataga Formation, Gulf of Alaska. Geological Society of America Bulletin 110 (3), 395–408.

Eyles, C.H., Eyles, N., Lagoe, M.B., 1991. The Yakataga formation: A late Miocene to Pleistocene record of temperate glacial marine sedimentation in the Gulf of Alaska. In: Anderson, J.B., Ashley, G.M. (Eds.), Glacial Marine Sedimentation: Paleoclimatic Significance. Geological Society of America, Boulder, pp. 159–180.

Gilchrist, A.R., Summerfield, M.A., Cockburn, H.A.P., 1994. Landscape dissection, isostatic uplift, and the morphologic development of orogens. Geology 22 (11), 963–966.

Hallet, B., 1979. A theoretical model of glacial abrasion. Journal of Glaciology 17, 209–221.

Hallet, B., Hunter, L., Bogen, J., 1996. Rates of erosion and sediment evacuation by glaciers: a review of field data and their implications. Global and Planetary Change 12, 213–235.

Hamilton, T.D., 1994. Late Cenozoic glaciation of Alaska. In: Plafker, G., Berg, H.C. (Eds.), The Geology of Alaska. Geological Society of America, Boulder, pp. 813–844.

Harbor, J., Warburton, J., 1993. Relative rates of glacial and nonglacial erosion in alpine environments. Arctic and Alpine Research 25, 1–7.

Harbor, J.M., 1992. Numerical modelling of the development of U-shaped valleys by glacial erosion. Geological Society of America Bulletin 104, 1364–1375.

Hostetler, S.W., Clark, P.U., 1997. Climatic controls of western U.S. glaciers at the last glacial maximum. Quaternary Science Reviews 16, 505–511.

Hudson, T., Plafker, G., Rubin, M., 1976. Uplift rates of marine terrace sequences in the Gulf of Alaska. In: Cobb, E.H. (Ed.), The United States Geological Survey in Alaska: Accomplishments during 1975. United States Geological Survey, Denver, pp. 11–13.

Huerta, A.D., Royden, L.H., Hodges, K.V., 1996. The interdependence of deformational and thermal processes in mountain belts. Science 273, 637–639.

Humphrey, N.F., Raymond, C.F., 1994. Hydrology, erosion and sediment production in a surging glacier: Variegated Glacier. Journal of Glaciology 40, 539–552.

Imbrie, J., Hays, J.D., Martinson, D.G., Mclntyre, A., Mix, A.C., Morley, J.J., Pisias, N.G., Prell, W.L., Shackleton, N.J., 1984. The orbital theory of Pleistocene climate: support from a revised chronology of the marine ∂O^{18} record. In: Berger, A.L.E.A. (Ed.), Milankovitch and Climate, Part 1. D. Reidel, Hingham, MA, pp. 269–305.

Koons, P., 1994. Three-dimensional critical wedges: tectonics and topography in oblique collisional orogens. Journal of Geophysical Research 99 (B6), 12301–12315.

Koons, P., 1998. Big mountains, big rivers, and hot rocks: Beyond isostacy. EOS, Transactions of the American Geophysical Union 79, F908.

Koons, P.O., 1995. Modelling the topographic evolution of collisonal belts. Annual Reviews of Earth and Planetary Sciences 23, 375–408.

Lagoe, M.B., Eyles, C.H., Eyles, N., Hale, C., 1993. Timing of late Cenozoic tidewater glaciation in the far North Pacific. Geological Society of American Bulletin 105, 1542–1560.

Lahr, J.C., Plafker, G., 1980. Holocene Pacific–North American plate interaction in southern Alaska: implications for the Yakataga seismic gap. Geology 8, 483–486.

Lundgren, P., Saucier, F., Palmer, R., Langon, M., 1995. Alaska crustal deformation: finite element modelling constrained by geologic and very long baseline interferometry data. Journal of Geophysical Research 100, 22033–22045.

Mann, D.H., 1986. Wisconsin and Holocene glaciation of southeast Alaska. In: Hamilton, T.D., Reed, K.M., Thorson, R.M. (Eds.), Glaciation in Alaska: The Geologic Record. Alaska Geologic Society, Anchorage, Alaska, pp. 237–265.

Mann, D.H., Ugolini, F.C., 1985. Holocene glacial history of the Lituya District, southeast Alaska. Canadian Journal of Earth Sciences 22, 913–928.

Masek, J.G., Isacks, B., Gubbels, T.L., Fielding, E.J., 1994. Erosion and tectonics at the margins of continental plateaus. Journal of Geophysical Research 99, 13941–13956.

Mayo, L.R., 1986. Annual runoff rate from glaciers in Alaska: a model using the altitude of glacier mass balance equilibrium. In: Kane,

D.L. (Ed.), Cold Regions Hydrology Symposium. American Water Resources Association, Bethesda, pp. 509–517.
Meigs, A., 1998. Bedrock landsliding forced by deglaciation: three possible examples from the Chugach/St. Elias Range, Alaska. EOS, Transactions of the American Geophysical Union 79, F337.
Mercer, J.H., 1960. The response of fjord glaciers to changes in the firnm limit. Journal of Glaciology, 850–858.
Miller, D.J., 1961. Geology of the Yakutat District, Gulf of Alaska Tertiary Province. Alaska. U.S. Geological Survey Open File Report, 61–103.
Molnar, P., 1987. Inversion of profiles of uplift rates for the geometry of dip-slip faults at depth, with examples from the Alps and the Himalaya. Annales Geophysicae 6, 663–670.
Molnar, P., England, P., 1990. Late Cenozoic uplift of mountain ranges and global climatic changes: chicken or egg? Nature 346, 29–34.
Molnia, B.F., 1986. Glacial history of the northeastern Gulf of Alaska — a synthesis. In: Hamilton, T.D., Reed, K.M., Thorson, R.M. (Eds.), Glaciation in Alaska: The Geologic Record. Alaska Geologic Society, Anchorage, Alaska, pp. 219–235.
O'Sullivan, P.B., Currie, L.D., 1996. Thermotectonic history of Mt. Logan, Yukon Territory Canada. Earth and Planetary Science Letters 144, 251–261.
O'Sullivan, P.B., Plafker, G., Murphy, J.M., 1997. Apatite fission-track thermotectonic history of crystalline rocks in the northern St. Elias Mountains, Alaska. In: Domouling, J.A., Gray, J.E. (Eds.), Geological studies in Alaska by the U.S. Geological. Survey, 1995. Reston, United States Geological Survey, pp. 283-293.
Østrem, G., 1972. Height of the glaciation level in northern British Columbia and southeastern Alaska. Geografiska Annaler 54A (2), 76–84.
Østrem, G., Haakensen, N., Eriksson, T., 1981. The glaciation level in southern Alaska. Geografiska Annaler 63A, 251–260.
Page, R.A., Stephens, C.D., Lahr, J.C., 1989. Seismicity of the Wrangell and Aleutian Wadati-Benioff zones and the North American plate along the Trans-Alaska Crustal transect, Chugach Mountains and Cooper River basin, southern Alaska. Journal of Geophysical Research 94, 16059–16802.
Paterson, W.S.B., 1994. The Physics of Glaciers. Elsevier, Tarrytown, 480 pp.
Péwé, T.L., 1975. Quaternary Geology of Alaska. United States Geological Survey Professional Paper, 145 pp.
Pfeffer, W.R., Sassolas, C., Bahr, D.B., Meier, M.F., 1998. Response time of glaciers as a function of size and mass balance: 2. Numerical experiments. Journal of Geophysical Research 103 (B5), 9783–9789.
Plafker, G., 1987. Regional geology and petroleum potential of the northern Gulf of Alaska continental margin. In: Scholl, D.W., Grantz, A., Vedder, J.G. (Eds.), Geology and Petroleum Potential of the Continental Margin of Western North America and Adjacent Ocean Basins-Beaufort Sea to Baja California. Texas, Circum-Pacific Council for Energy and Mineral Resources. Earth Science Series, Houston, TX, pp. 229–268.
Plafker, G., Gilpin, L.M., Lahr, J.C., 1994a. Neotectonic map of Alaska. In: Plafker, G., Berg, H.C. (Eds.), The Geology of Alaska: The Geology of North America. Geological Society of America, Boulder.
Plafker, G., Hudson, T., Richter, D.H., 1977. Preliminary observations on late Cenozoic displacements along the Totschunda and Denali fault systems. In: Blean, K.M. (Ed.), Geologic Studies in Alaska by the U.S. Geological Survey During 1976. Geological Survey, Reston US, pp. B67–B69.
Plafker, G., Hudson, T.L., Bruns, T.R., Rubin, M., 1978. Late Quaternary offsets along the Fairweather fault and crustal plate interactions in southern Alaska. Canadian Journal of Earth Sciences 15 (5), 805–816.
Plafker, G., Hudson, T., Rubin, M., Dixon, K.L., 1982. Holocene marine terraces and uplift history in the Yakataga seismic gap near Icy Cape. Alaska. U.S. Geological Survey Circular 844, 111–115.
Plafker, G., Moore, J.C., Winkler, G.R., 1994b. Geology of the southern Alaska Margin. In: Plafker, G., Berg, H.C. (Eds.), The Geology of Alaska: The Geology of North America. Geological Society of America Boulder, pp. 389-449.
Porter, S.C., 1975. Glaciation limit in New Zealand's Alphs. Arctic and Alpine Research 7 (1), 33–37.
Porter, S.C., 1977. Present and past glaciation threshold in the Cascade Range, Washington, U.S.A.: topographic and climatic controls and paleoclimatic implications. Journal of Glaciology 18 (78), 101–116.
Porter, S.C., 1988. Landscapes of the Last Ice Age in North America. In: Carlisle, R.C. (Ed.), American Before Columbus: Ice-Age Origins, Ethnology Monographs. University of Pittsburgh, Pittsburgh, pp. 1–24.
Porter, S.C., 1989a. Late Holocene fluctuations of the fjord glacier system in Icy Bay Alaska. Arctic and Alpine Research 21 (4), 364–379.
Porter, S.C., 1989b. Some geological implications of average Quaternary glacial conditions. Quaternary Research 32 (3), 245–261.
Porter, S.C., Pierce, K.L., Hamilton, T.D., 1983. Late Wisconsin mountain glaciation in the western United States. In: Porter, S.C. (Ed.), The Late Pleistocene: Late Quaternary Environments of the United State. University of Minnesota Press, Minneapolis, pp. 71–111.
Powell, R.D., 1983. Glacial-marine sedimentation processes and lithofacies of temperate tidewater glaciers, Glacier Bay Alaska. In: Molnia, B.F. (Ed.), Glacio-marine Sedimentation. Plenum Press, New York, pp. 185–232.
Raymo, M.E., Ruddiman, W.F., 1992. Tectonic forcing of late Cenozoic climate. Nature 359, 117–122.
Royden, L., 1993. The steady state thermal structure of eroding orogenic belts and accretionary prisms. Journal of Geophysical Research 98, 4487–4507.
Sauber, J., McClusky, S., King, R., 1997. Relation of ongoing deformation rates to the subduction zone processes in southern Alaska. Geophysical Research Letters 24 (22), 2853–2856.
Sauber, J., Plafker, G., Molnia, B., Bryant, M., 1999. Crustal deformation associated with elevation changes associated with glacial fluctuations in the eastern Chugach Mountains, Alaska. Journal of Geophysical Research.
Schmidt, K.M., Montgomery, D.R., 1995. Limits to relief. Science 270, 617–620.
Seeber, L., Gornitz, V., 1983. River profiles along the Himalayan arc as indicators of active tectonics. Tectonophysies 92, 335–367.
Seeber, L., Pecher, A., 1998. Strain partitioning along the Himalayan arch and Nanga Parbat antiform. Geology 26 (9), 791–794.
Sidle, R.C., Milner, A.M., 1989. Stream development in Glacier Bay National Park. Alaska, U.S.A. Arctic and Alpine Research 21 (4), 350–363.
Tarr, R.S., 1909. The Yakutat Bay region, Alaska, physiography and glacial geology, U.S. Geological Survey Professional Paper, pp. 183.
Tarr, R.S., 1914. In: Alaska Glaciological Studies. National Geographic Society, Washington, DC, 498 pp.
Tarr, R.S., Martin, L., 1912. Earthquakes at Yakutat Bay, Alaska, in September 1899. U.S. Geological Survey Professional Paper, p. 133.
Tucker, G.E., Bras, R., 1998. Hillslope processes, drainage density, and landscape morphology. Water Resources Research 34 (10), 2751–2764.
Whipple, K.X., Kirby, E., Brocklehurst, S.H., 1999. Geomorphic limits to climatically induced increases in topographic relief. Nature 401, 39–43.
Whipple, K.X., Tucker, G.E., 1999. Dynamics of the stream-power river incision model: implications for height limits of mountain ranges, landscape response timescales, and research needs. Journal of Geophysical Research, 17661–17674.
Willett, S., Beaumont, C., Fullsack, P., 1993. Mechanical models for the tectonics of doubly vergent compressional orogens. Geology 21, 371–374.

Williams, D.F., Thunnell, R.C., Tappa, E., Rio, D., Raffi, I., 1988. Chronology of the Pleistocene oxygen isotope record: 0-1.88 m.y. B.P. Paleogeography. Palaeoclimatology, Paleoecology 64, 221–240.

Zeitler, P.K., 1985. Cooling history of the NW Himalaya. Pakistan. Tectonics 4 (1), 127–151.

Zeitler, P.K., Koons, P.O., 1998. Nanga Parbat as tectonic aneurysm: a metamorphic signature of indentor-corner dynamics. EOS, Transactions of the American Geophysical Union 79, F910.

Zeitler, P.K., Sutter, J.F., Williams, I.S., Zartman, R., Tahirkheli, R.A.K., 1989. Geochronology and temperature history of the Nanga Parbat-Haramosh Massif, Pakistan. In: Malinconico, L.L., Lillie, R.J. (Eds.), Tectonics of the Western Himalaya. Geological Society of America, Boulder, pp. 1–22.

Zeitler, P.K., Tahirkheli, R.A.K., Naeser, C.W., Johnson, N.M., 1982. Unroofing history of a suture zone in the Himalaya of Pakistan by means of fission-track annealing ages. Earth and Planetary Science Letters 57, 227–240.

Zhang, W.H., Montgomery, D.R., 1994. Digital elevation model grid size, landscape representation, and hydrologic simulations. Water Resources Research 30, 1019–1028.